0016-0032(95)00023-2

Bifurcation of Power Electronic Circuits†

by DENISE M. WOLF, MATTHEW VARGHESE *and* SETH R. SANDERS

Department of Electrical Engineering and Computer Sciences, University of California, Berkeley CA 94720, U.S.A.

ABSTRACT: *This paper studies various bifurcations of periodic orbits in power electronic circuits: cyclic fold bifurcations, period-doubling bifurcations, and bifurcations due to Poincaré map discontinuities. We focus on circuits operating under closed-loop control and/or containing nonlinear reactive components. Section III contains an exploration of cyclic fold bifurcations and the associated resonant jump phenomenon in circuits containing saturable reactors. Section IV gives a comprehensive overview of period-doubling phenomena in closed-loop DC–DC conversion circuits. We study circuits with homeomorphic and unimodal Poincaré maps, those that period-double a single time and those that period-double repeatedly in a cascade to chaos. This section ends with a result relating non-genericity of a period-doubling bifurcation to half-wave orbital symmetry. An interesting feature of power electronic circuits is that they may have Poincaré maps that are continuous but not everywhere differentiable, or discontinuous. In Section V we study, in detail, bifurcation behavior in a thyristor controlled VAR compensator, understood in terms of Poincaré map discontinuities. We show that Poincaré map discontinuities are due to jumps in circuit switching times. We show how map discontinuities lead to steady state jump phenomena, and distinguish between transient behavior related to switch time jumps and steady state bifurcations. The paper ends with an Appendix, in which concepts underlying cyclic fold bifurcations for the case of a continuous but not everywhere differentiable map are developed.*

I. Introduction

Power electronic circuits are designed to process electrical energy, in contrast to the function of processing signals in many other circuits used in various branches of electrical engineering. Power electronic circuits in some form are used in virtually all types of electrical equipment, ranging from multi-megawatt power systems applications to milliwatt battery management circuitry. The function of a power electronic circuit is to condition and control the flow of electrical energy. Specifically, this may mean to interface between AC and DC systems, change frequency in AC–AC conversion applications, provide electrical isolation, and provide voltage, current, and impedance matching. The most familiar circuits for providing voltage matching are the ubiquitous DC–DC converters. In the highest power applications used in utility systems, example circuits are static VAR compensators and rec-

† This work was supported by SRC contract 95-DC-324, Electric Power Research Institute contract RP8018-08, and NSF grant ECS-9358284.

Pergamon

tifier/inverter interfaces with high voltage DC (HVDC) transmission lines. At lower, but still substantial power ratings, power electronic circuits are used extensively in variable speed motor/generator control systems, in lighting systems, in photovoltaic interfaces, in welding, and in induction heating applications.

Since the aim is to process energy, efficiency is usually of a primary concern. The reasons for this are twofold. First, the cost of energy may dictate a high efficiency solution. Examples occur in utility applications, battery powered and especially portable equipment, and aerospace applications among others. Second, whenever energy is processed inefficiently, heat is generated. The need to remove excess heat provides a premium on high efficiency operation in virtually all applications.

Since power electronic circuits are designed to process energy efficiently, these circuits are designed with nominally lossless circuit elements. The circuit elements comprising a power electronic circuit include switches, implemented with transistors, diodes, and thyristors, and reactive components including inductors, transformers, and capacitors. Depending on one's point of view, motors and/or generators may also be viewed as viable circuit elements since these devices may be viewed as transformers interfacing the mechanical and electrical domains. Devices that are not included in power electronic circuits are resistive devices, including transistors operating in their active regions. As such, linear voltage regulators and classical power amplifiers are not viewed as power electronic circuits, here.

It is the very nature of a circuit built from switches and reactive components, and designed to operate to process power that is of interest here. In the early work of Duffin (**1**), necessary conditions for the conversion of DC power to AC power were established. In particular, the article (**1**) applied Tellegen's theorem and concepts of passivity and incremental passivity to establish that at least one incrementally active resistance must be present in the *DC network* of a power conversion circuit. Here, the DC network is defined as the network obtained by open-circuiting capacitors and eliminating branches in series with the capacitors, and by short-circuiting inductors and combining the nodes to which each inductor is connected. This result was extended in the work of Wolaver (**2**). We summarize some of these results in the following discussion.

To begin, we introduce some of the terminology from (**2**) for a circuit operating in the steady state. Let each branch variable (i.e. branch current and branch voltage) be represented as the sum of a constant time-averaged component and a zero-mean time-varying component. For instance, a branch voltage can be expressed in the form

$$v(t) = \bar{v}+\tilde{v}(t), \tag{1}$$

where $\bar{v}$ is the (constant) time-averaged value of the voltage and $\overline{\tilde{v}(t)} = 0$. A branch element in the converter is termed *DC active* if it supplies *average DC power* in the steady state, i.e.

$$\bar{v}\bar{i} < 0.$$

Note that an element that is DC active does not necessarily supply any average real power to the rest of the circuit. A branch element is termed *AC active* if it supplies *average AC power*, i.e.

$$\overline{\tilde{v}\tilde{i}} = \overline{(v-\bar{v})(i-\bar{i})} = \overline{vi}-\bar{v}\bar{i} < 0.$$

Among the results obtained in (**2**) is the fact that every DC–DC conversion circuit formed from interconnections of two-terminal devices must contain at least two nonlinear and/or time-varying resistances. In particular, one of these must be DC active to supply average power to the load. This element is often a diode. The other nonlinear/time-varying resistance must be AC active to convert power from the DC source to AC power which in turn can be rectified by the DC active resistance. The second nonlinear/time-varying resistance is often a controlled switch such as a transistor. The necessity of an AC active resistance is equivalent to the result stated by Duffin (**1**).

In nearly all modern power conversion circuits, the AC active and DC active elements are transitors, diodes, or thyristors. Because of the relative simplicity of periodic steady states, as opposed to alternatives, nearly all modern power conversion circuits are designed to operate in a periodic steady state. Notable exceptions occur in circuits that interface with AC systems where the normal steady state may usually be termed *almost periodic*. The periodicity is typically imposed by a clocked control circuit, an AC source, or in some other cases by the autonomous behavior of the circuit. Because of this periodicity, our focus in this paper is on periodic steady state operation of these circuits. As such, we develop the necessary mathematical tools—Poincaré maps and their properties for studying the dynamics of these nominally periodic circuits. Specifically, Section II gives mathematical preliminaries on this for the remainder of the paper.

The rest of the paper is a study of the type and genericity of various bifurcations of periodic orbits in power electronic circuits. Although some simple reasoning (**3**) leads one to conclude that a switched circuit built from incrementally passive resistors, linear reactive elements, and ideal switches will exhibit a unique steady state under open-loop operation and some mild topological conditions, our focus is on circuits operating under closed-loop control and/or containing nonlinear reactive components.

Section III studies cyclic fold bifurcations and the associated resonant jump phenomenon in circuits containing saturable reactors. The tools from classical bifurcation theory that require differentiability of the Poincaré map appear to be adequate for these examples. Section IV gives a comprehensive overview of period-doubling phenomena in closed-loop DC–DC conversion circuits. A substantial body of literature on this topic has emerged, and this section attempts to unify the literature with the theory, again based on differentiable Poincaré maps.

In Section V we study, in detail, bifurcation behavior in a thyristor controlled VAR compensator. The tools needed for understanding the dynamics in this example are substantially different from that available in the classical literature on bifurcation theory. In particular, the Poincaré map arising in this example is neither differentiable nor continuous. In fact, bifurcations exist because of the nature of the implicitly controlled switch transitions in this circuit. We give a comprehensive analysis of the phenomenon.

Vol. 331B, No. 6, pp. 957–999, 1994

II. Mathematical Preliminaries

In this section we define Poincaré maps for autonomous and non-autonomous nonlinear dynamical systems, and describe typical Poincaré map derivations for power electronic circuits. The significance of Poincaré map fixed points and the eigenvalues of the linearized map at a fixed point are also discussed.

Sampling in switched circuits. Switched circuits in power electronics operate in cyclic fashion. Systems that have periodic solutions are usually analyzed by the Poincaré map, which is a suitably chosen transverse hyperplane to trajectories of the corresponding continuous time system. Conceptually, the Poincaré map is obtained by sampling the system trajectory as it intersects the hyperplane. Thus, a Poincaré map is a form of discretization of a continuous time system.

Defining the Poincaré map. Consider an autonomous differential equation $\dot{x} = f(x)$, $x \in \mathbb{R}^n$. Denote its solution starting at x at time $t = 0$ by $\phi_t(x) = \phi(t, x)$. The map $\phi : (t, x) \to \phi(t, x)$ is called the *flow* of the vector field $f(x)$. Let Γ be a periodic orbit of period T of the flow ϕ. We first take a local cross section $S \subset \mathbb{R}^n$, of dimension $n-1$, such that (i) the flow ϕ is everywhere transverse† to S, and (ii) S intersects Γ at a unique point p.‡ Let $\mathcal{U} \subset S$ be a neighborhood of p. For $q \in \mathcal{U}$ the *first return* or *Poincaré* map $P : \mathcal{U} \to S$ is defined by

$$P(q) := \phi_{\tau(q)}(q) = \phi(\tau(q), q)$$

where $\tau(q)$ is the time it takes for the orbit based at q to first return to S. Thus $\tau(p) = T$ and $\tau(q) \to T$ as $q \to p$. Also, p is a fixed point of P. In local coordinates, P is a map from $\mathcal{U} \subset \mathbb{R}^{n-1}$ to $\mathbb{R}^{n-1}$, so $DP(p)$ has $n-1$ eigenvalues, called the *Floquet multipliers* (or characteristic multipliers) associated with the periodic orbit Γ.

For *non-autonomous* systems, a Poincaré map may be defined by sampling the system flow $\phi_t(x) = \phi(t, x)$ of the periodically forced system $\dot{x} = f(x, t) = f(x, t+T)$ every T seconds, for a first return $P(q) := \phi_T(q) = \phi(T, q)$.

A periodic orbit Γ is asymptotically stable if and only if all the Floquet multipliers have magnitude less than 1. Consequently, p is a stable fixed point for the Poincaré map if and only if Γ is stable.

III. Cyclic Fold Bifurcations

Suppose a parameterized continuous time system has a T-periodic orbit Γ_1 with trajectory $x_1(t) = x_1(t+T)$, and another T-periodic orbit Γ_2 with trajectory $x_2(t) = x_2(t+T)$. The system undergoes a cyclic fold bifurcation (CFB) if the two periodic orbits coalesce and then "disappear" as a parameter embedded in the

† This means the inner product $\langle f(x), n(x) \rangle \neq 0$ for all $x \in S$, where $n(x)$ is the normal to S at x.

‡Such a construction could result in a non-unique Poincaré map. In special cases, this non-uniqueness of construction could lead to different discrete time observations of bifurcations involving periodic orbits.

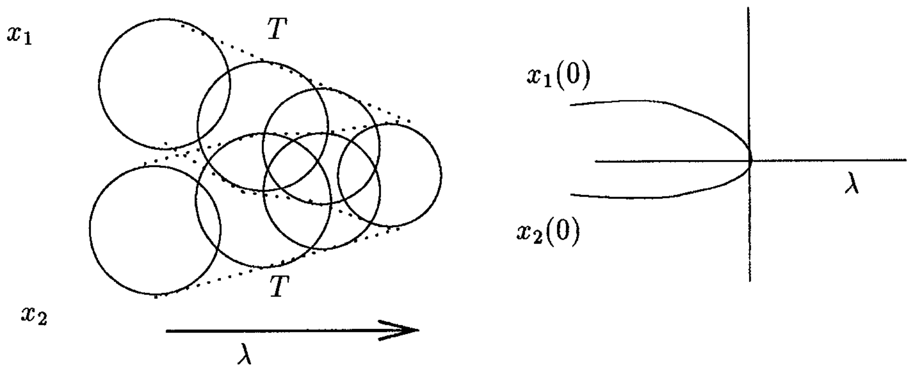

FIG. 1. (a) A cyclic fold bifurcation. Two real periodic orbits coalesce and disappear as a parameter is varied. (b) The corresponding folding fixed point path, with the orbits sampled at time $t = 0$, $x_1(0)$ and $x_2(0)$ serving as fixed points.

circuit equations is varied monotonically, as illustrated in Fig. 1(a). In the case of a differentiable Poincaré map, if one of the coalescing orbits is stable, then the other must be unstable, and if $n-1$ of a total of n Floquet multipliers lie within the unit circle, then a generic CFB must consist of two coalescing orbits of opposite stability. Other stability combinations are possible for Poincaré maps that are continuous but not everywhere differentiable, as will be shown in the Appendix. Cyclic fold bifurcations are considered generic to nonlinear dynamical systems (**4**), and have been observed in power electronic circuits such as the ferroresonant circuit example discussed in this section (**5**–**7**).

Because power electronic circuits contain state controlled switches, Poincaré maps of power electronic circuits are not necessarily everywhere differentiable. They may be everywhere differentiable, or continuous and piecewise differentiable, or even discontinuous, depending on the state feedback function controlling the switches, the discontinuities in the differential equations describing the circuit. Cyclic fold bifurcations may occur in circuits with differentiable, piecewise differentiable or discontinuous Poincaré maps. Because there are differences in the mathematical characterization and stability properties of cyclic fold bifurcations occurring in systems with these different types of Poincaré maps, the topic may be organized by Poincaré map class. We discuss differentiable Poincaré maps in this section. Continuous, but non-differentiable Poincaré maps are discussed in the Appendix.

3.1. *Cyclic folds—differentiable Poincaré maps*

Classical bifurcation theory mostly concerns itself with the bifurcations of differentiable Poincaré maps (**4**). If the point p_λ of the periodic orbit Γ_λ is a fixed point of the map P_λ ($p_\lambda = P_\lambda(p_\lambda)$), then the eigenvalues of the linearization of the differentiable map P_λ at p_λ, $\mu_i \in \mu(DP_\lambda(p_\lambda))$, reflect the stability of the fixed point p_λ and its corresponding periodic orbit Γ_λ. They also serve to determine the occurrence of a bifurcation.

As long as no eigenvalue is on the unit circle ($|\mu_i| \neq 1$, $\forall i$), the periodic orbit Γ_λ

Vol. 331B, No. 6, pp. 957–999, 1994

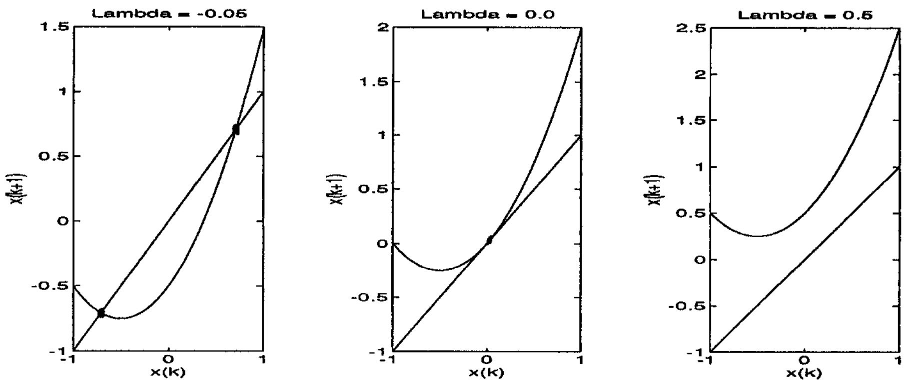

FIG. 2. CFB normal form $x_{k+1} = x_k + x_k^2 + \lambda$ for various λ. (a) At $\lambda = -0.5$, there are two solutions, one stable and the other unstable. (b) At $\lambda = 0$ the two solutions coalesce in a CFB. (c) At $\lambda = 0.5$, the map has no solutions.

is hyperbolic and non-bifurcating. However, when $|\mu_i| = 1$, the periodic orbit undergoes some type of bifurcation. A *cyclic fold bifurcation* of a differentiable Poincaré map corresponds to a single eigenvalue $\mu_i \in \mu(DP_\lambda)$ passing through $+1$ transversally.

If an eigenvalue $\mu_i = 1$ at a fixed point p_λ of P_{λ_0}, then the matrix $DP_{\lambda_0}(p_{\lambda_0}) - I$ is not invertible, where I is the identity matrix. So we cannot apply the implicit function theorem to get a smooth fixed point solution $p(\lambda)$ in the neighborhood of p_{λ_0}. Indeed the fixed point solution undergoes a saddle-node bifurcation at λ_0. Hence a cyclic fold bifurcation of periodic orbits corresponds to a (local) saddle-node bifurcation of the fixed point solution for the Poincaré map, a *folding fixed point path*, as shown in Fig. 1(b).

Geometry-normal form

A normal form, or simplest, one-dimensional representation of a differentiable Poincaré map $x_{k+1} = P_\lambda(x_k)$ in the neighborhood of a cyclic fold bifurcation is as follows (**4**):

$$x_{k+1} = x_k + x_k^2 + \lambda. \tag{2}$$

Figures 2(a)–(c) show MATLAB plots of this map at different values of λ: $\lambda = -0.5$, $\lambda = 0.0$ and $\lambda = 0.5$.

A point p_λ is a fixed point of the map P_λ if $p_\lambda = P_\lambda(p_\lambda)$. The fixed points of the map $x_{k+1} = x_k + x_k^2 + \lambda$ at different values of λ may be seen in Figs 2(a)–(c). These fixed points satisfy the equations $x_{k+1} = x_k + x_k^2 + \lambda$ and $x_{k+1} = x_k$, which reduce to the equation $p_\lambda^2 + \lambda = 0$. Graphically, fixed points are the intersections of the function $x_k + x_k^2 + \lambda$ and the diagonal $x_{k+1} = x_k$. Examining Figs 2(a)–(c) or the fixed point equation $p_\lambda^2 + \lambda = 0$ reveals that the normal form may have two real fixed point solutions for $\lambda < 0$, no real fixed point solutions for $\lambda > 0$, or one real solution for $\lambda = 0$. For example, at $\lambda = -0.5$ there are two fixed points labeled $p1_\lambda$ and $p2_\lambda$ in Fig. 2(a). One of these fixed points, $p1_\lambda$, is stable, and the other, $p2_\lambda$, is

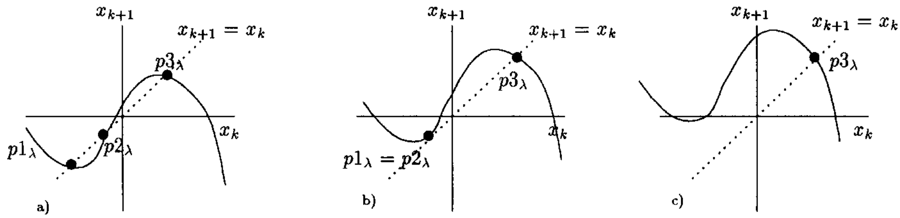

FIG. 3. Jump phenomena for differentiable maps. (a) The differentiable map has three orbits, two stable and one unstable. (b) The differentiable map undergoes a cyclic fold bifurcation, and two orbits, $p1$ and $p2$, coalesce. (c) Upon the cyclic fold bifurcation, if the state trajectory was in a steady state $p1$, it will *jump* to the remaining stable orbit, $p3$.

unstable. The stability of a fixed point is determined by the slope of the Poincaré map at the fixed point, which is also the magnitude of the eigenvalue of the linearized Poincaré map. The slope of the normal form at p_λ is $1+2p_\lambda$, so p_λ is stable if $|1+2p_\lambda|$ is less than one, and unstable if $|1+2p_\lambda|$ is greater than one.

As λ is increased from $\lambda = -0.5$ to $\lambda = 0$, the two fixed points approach one another to coalesce into a double root $p1_\lambda = p2_\lambda = 0$ at $\lambda = 0$. This is the *cyclic fold bifurcation* point. Figure 2(b) shows the normal form at the cyclic fold bifurcation point, $\lambda = 0$.

For parameter values $\lambda > 0$, the fixed point equation $p_\lambda^2 + \lambda = 0$ has no real solutions. The function does not intersect the diagonal and the map has no fixed points, as shown in Fig. 2(c) for $\lambda = 0.5$.

Observe in Fig. 2(b) that the slope of the function, or eigenvalue of the linearized map, is $+1$ at the cyclic fold bifurcation point (at $p1_\lambda = p2_\lambda = 0$, slope $1+2p_\lambda = 1$). For a differentiable map, the only way two orbits can coalesce is if the map becomes tangent to the diagonal at a double root. It is this tangency of the function to the diagonal that leads to the 'slope equals one' cyclic fold bifurcation condition. Thus, *differentiability* of the map is fundamentally connected with the classical fold bifurcation.

Also, for first order systems differentiability requires that a cyclic fold bifurcation join a stable and an unstable orbit. Since the slope/eigenvalue of the map approaches $+1$ at a cyclic fold bifurcation point, it must be greater than $+1$ at one of the coalescing fixed points, and less than $+1$ at the other. This corresponds to an encroaching union of a stable orbit and an unstable orbit. For higher order systems with $n-1$ of a total of n eigenvalues within the unit circle, an analogous argument applies.

Jump phenomena

Figures 3(a)–(c) illustrate typical jump phenomena of circuits with differentiable Poincaré maps. Figure 3(a) shows a differentiable Poincaré map with three fixed points, $p1_\lambda$, $p2_\lambda$, and $p3_\lambda$, two stable ($p1_\lambda, p3_\lambda$) and one unstable ($p2_\lambda$). As the parameter λ is increased, the fixed points $p1_\lambda$ and $p2_\lambda$ coalesce in a cyclic fold bifurcation, as shown in Fig. 3(b). For parameter values beyond the CFB point, the map has just one fixed point, $p3_\lambda$.

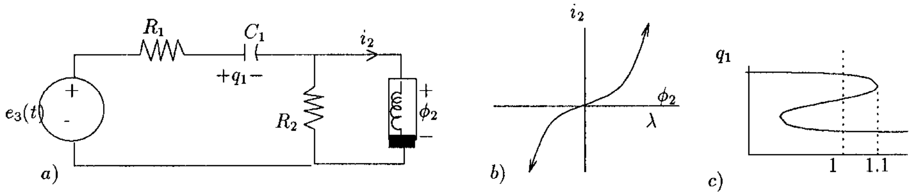

FIG. 4. (a) Ferroresonant circuit. (b) Nonlinear inductor characteristic. (c) Fixed point curve as a function of λ.

If the circuit happens to be operating in the stable steady state associated with the fixed point $p1_\lambda$, then varying the circuit parameter λ through a range of values including the CFB value results in the circuit trajectory *jumping* to a new stable orbit, $p3_\lambda$. This jump is signaled by an eigenvalue of the linearized Poincaré map approaching $\mu = +1$ as the CFB nears, and, when the two-point boundary value problem defining the periodic orbits of a circuit has been algebraically formulated, by ill-conditioning of the equations in the neighborhood of the bifurcation.

Next, we introduce an example of a power electronic circuit that exhibits cyclic fold bifurcations and that can exhibit jump phenomena. This circuit has a differentiable Poincaré map, as discussed here.

Circuit example (ferroresonant)

Nearly all practical inductors and transformers are built with windings on magnetic cores that exhibit magnetic saturation. As such, these devices are inherently nonlinear. In a number of applications, these devices are designed to operate in saturation, as well as in their linear regimes. Examples are in magnetic amplifier circuits and in regulating transformers. The example of Fig. 4(a) studied in (**5–7**) is derived from an application where a saturable reactor forms a nonlinear resonant circuit with a capacitor. Although this example is constructed to exhibit the interesting nonlinear phenomena of fold bifurcations and the associated jump resonance, it contains the elements present in many more practical scenarios.

This ferroresonant circuit has *state equations*

$$(R_1+R_2)\dot{q}_1 = -q_1/C_1+R_2 g(\phi_2)+e_3(t)$$
$$(R_1+R_2)\dot{\phi}_2 = -R_2 q_1/C_1-R_1 R_2 g(\phi_2)+R_2 e_3(t)$$

where states q_1 and ϕ_2 are the charge across the capacitor and the flux through the inductor, respectively. The nonlinear inductor characteristic is $i_2 = g(\phi_2) = a\phi_2+b\phi_2^3$, as shown in Fig. 4(b), and the sinusoidal forcing function is $e_3(t) = \lambda E \cos wt$. For the state vector $x = (q_1, \phi_2)$ we refer to the above state equations as $\dot{x} = f_\lambda(x, t)$. We parameterize the circuit by multiplying the forcing function by a parameter λ to get $e_3(t) = \lambda E \cos wt$. In this example, bifurcations of T-periodic orbits with the variation of the parameter λ are of interest.

Because the function f_λ is periodic with period $T = w/(2\pi)$, we may define a *Poincaré map* by sampling the system flow every T seconds. If the system flow is $x(t) = \phi(t, x(t_0), t_0, \lambda)$, then the Poincaré map $P_\lambda: \mathbb{R}^2 \to \mathbb{R}^2$ is given by the equation

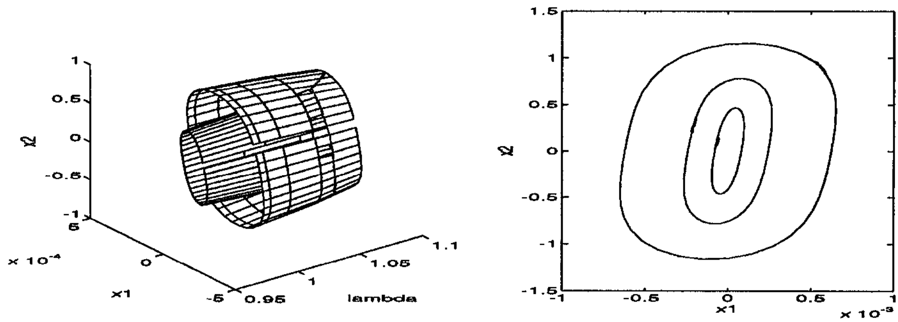

FIG. 5. (a) A stable and an unstable orbit coalesce in a cyclic fold bifurcation as λ is varied. (b) Three periodic orbits at the same value of λ ($\lambda = 1$). The center orbit is unstable, and the two outer ones are stable.

$x_{k+1} = x((k+1)T) = \phi((k+1)T, x(kT), t_0, \lambda) = P_\lambda(x_k)$, $k \in \mathbb{Z}_+$. For a given parameter value λ, any T-periodic orbit of the circuit has a corresponding fixed point x of the Poincaré map P_λ.

The folding solution path of orbits, corresponding to values of λ at which the circuit has first one, then three, and then one T-periodic solution (**5**–**7**), is represented in Fig. 4(c) for the circuit values $R_1 = 50\Omega$, $R_2 = 10\Omega$, $C_1 = 1.69\mu$F, $E = 100$V and $(a, b) = (0.03,\ 0.174)$. A finite difference formulation with the Trapezoidal Rule is employed in a MATLAB program with $N = 40$, where N is the number of uniform sample points of the orbit (**8**). The three orbits at $\lambda = 1$ are illustrated in Fig. 5(b). The two outer orbits, Γ_1 and Γ_3, are stable, and the center orbit Γ_2 is unstable. Figure 5(a) shows a MATLAB mesh plot of the *cyclic fold bifurcation* occurring at $\lambda \approx 1.1$, at which point the small stable orbit Γ_1 coalesces with the unstable orbit Γ_2. An eigenvalue of the Poincaré map approaches 1 at the bifurcation, and the finite difference formulation becomes ill-conditioned, as shown in Fig. 6(b).

Figure 6(a) illustrates the *jump phenomenon* related to the presence of a cyclic

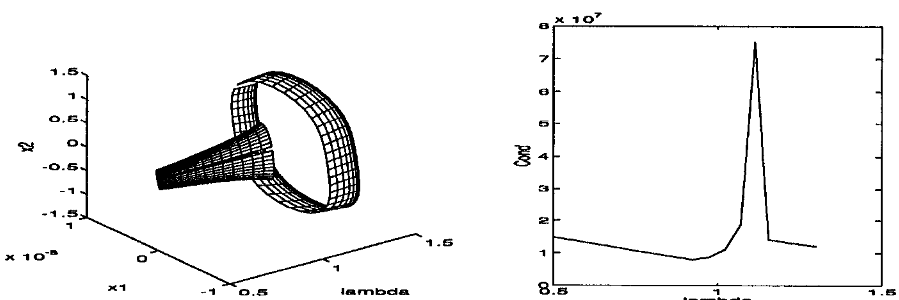

FIG. 6. (a) Stable periodic orbit as a function of λ. The jump from the stable periodic orbit Γ_0 to the stable periodic orbit Γ_2 is due to the presence of a cyclic fold bifurcation at $\lambda \approx 1.1$. (b) Conditioning as a function of λ, reflecting the cyclic fold bifurcation and associated jump phenomenon.

Vol. 331B, No. 6, pp. 957–999, 1994

fold bifurcation, as discussed previously. If the circuit is operating in a steady state corresponding to the stable orbit Γ_1, and then the parameter λ is gradually increased to a value greater than λ^*, where $\lambda^* \approx 1.1$ is the parameter value at which the orbit undergoes a cyclic fold bifurcation, then the circuit will exhibit jump behavior and the trajectory will "jump" from a continuation of Γ_1 to a continuation of Γ_3, as shown in Fig. 6(a).

As discussed in (**5–7**), ferroresonant circuits exhibit a variety of bifurcations other than the cyclic folds discussed in this example, and other nonlinear behaviors including chaotic waveforms.

This section deals with the case of power electronic circuits with differentiable Poincaré maps that undergo cyclic fold bifurcations. For a discussion of cyclic fold bifurcations of circuits with continuous but non-differentiable Poincaré maps, see the Appendix. The next section presents period-doubling bifurcations in power electronic circuits, including conditions under which a circuit will period-double once and then not again, and conditions under which a circuit will period-double repeatedly along a path to chaos.

IV. Period-doubling Bifurcations

4.1. *An introduction to period-doubling*

Suppose a continuous time system has a stable periodic orbit Γ of period T, with state trajectory $x(t) = x(t+T)$. The periodic orbit is said to *period-double* if a monotonic variation of a circuit parameter gives rise to a stable periodic orbit of period $2T$ just as the periodic orbit of period T becomes unstable. Period-doubling is considered generic to nonlinear dynamical systems, and has been observed in power electronic circuits such as DC–DC converters.

In this section, we give an overview of period-doubling phenomena in closed-loop DC–DC conversion circuits with locally differentiable Poincaré maps. We draw from power electronics and bifurcation theory literature, and from our own analysis, to answer questions about when and why such circuits period-double, whether or not they period-double repeatedly to chaos, and the relationship between orbit symmetry and the likelihood of encountering a period-doubling bifurcation.

Subsection 4.2 begins by examining a power conversion circuit that period-doubles a single time with the variation of a circuit parameter, and invokes intuitive circuit-based arguments along with results on homeomorphic maps to explain why it does not period-double repeatedly. Then a technique typically used by circuit designers to avoid a period-doubling bifurcation, the inclusion of a ramp in the current mode control, is described and explained in terms of Poincaré map eigenvalues and the homeomorphic map slope.

Subsection 4.3 deals with DC–DC converters that appear to period-double repeatedly to chaos. We present the associated normal form, a simple one-dimensional dynamical system that exhibits a period-doubling cascade, to explain the phenomenon, and then present detailed power electronic circuit examples. These examples are second order buck converters operating in different modes. We emphasize the difference between circuits that period-double to chaos and those that period-double a single time.

In the final subsection, 4.4, we address the question of how likely a power electronic circuit is to period-double, and present results relating the genericity (or lack thereof) of period-doubling bifurcations to orbit symmetries.

First, we present a brief mathematical description of period-doubling for differentiable Poincaré maps.

Mathematical definition of period-doubling. The crossing of the unit circle at -1, by a Floquet multiplier predicts the occurrence of period-doubling. Suppose p_0 is a stable fixed point for P_{λ_0}. Furthermore assume that the map P_{λ_0} is everywhere differentiable. The implicit function theorem gives a smooth fixed point solution $\lambda \to p(\lambda)$ through (p_0, λ_0). At the period-doubling bifurcation, the solution branch loses its stability and a stable periodic orbit consisting of two periodic points† of period two is created. Let $p_1(\lambda)$, $p_2(\lambda)$ be the two period-two periodic points for the Poincaré map P_λ. Since $P_\lambda(p_1(\lambda)) = p_2(\lambda)$ and $P_\lambda(p_2(\lambda)) = p_1(\lambda)$, a new periodic orbit of *twice* the period is created, and it intersects the Poincaré section at $p_1(\lambda)$ and $p_2(\lambda)$. Thus, a period-doubling bifurcation corresponds to a (local) pitchfork bifurcation of the fixed point solution.

4.2. *A single period doubling*

In this subsection we define homeomorphic Poincaré maps and present a result on period-doubling for such maps. In brief, the result states that such a map can period-double at most a single time. Then we present an example of a DC–DC converter that undergoes a single period-doubling bifurcation with the variation of a parameter, the source voltage, and show that it has a homeomorphic Poincaré map and so cannot period-double again. This circuit is a first order buck converter under current mode control. Then we take the same circuit and show how adding a compensation ramp to the control can prevent the circuit from period-doubling over the parameter range of interest. This is a common design technique to prevent instabilities.

4.2.1. *Period-doubling for homeomorphic Poincaré maps.* Consider the case when the Poincaré map is a *homeomorphism* of $\mathbb{R}$. A function $f(x)$ is a *homeomorphism* if $f(x)$ is one-to-one, onto and continuous, and $f^{-1}(x)$ is also continuous.

An example of a homeomorphic Poincaré map is of the form $x_{k+1} = \lambda \mathrm{e}^{-(k_1+k_2x_k)} + k_3$, where the k_is are constants. A homeomorphic map like this one can period-double to at most prime period two with the variation of a parameter, as shown in Figs 7 and 8 for our example map. This result is stated more formally, and proved as follows.

Lemma H

A homeomorphism of $\mathbb{R}$ can have no periodic points with prime period greater than two.

†A periodic point of period n for a map f is a point x_0 which satisfies $f^n(x_0) = x_0$, where $f^n = f \circ \ldots \circ f$ (n times). If n is a period for x_0, then kn is also a period for x_0, $k = 1, 2, \ldots$. The smallest of all periods for x_0 is called the fundamental or prime period.

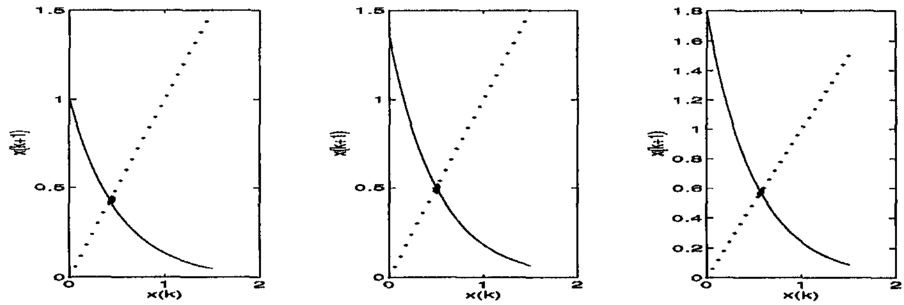

FIG. 7. A homeomorphic map of the form $x_{k+1} = \lambda e^{-(k_1+k_2x_k)}+k_3$. As the parameter λ is varied, the slope of the fixed point passes through -1, and the orbit period-doubles a single time.

Proof: Consider the following two scenarios: (a) The slope of $f(\cdot)$ is everywhere positive, or (b) the slope of $f(\cdot)$ is everywhere negative. We do not need to consider any other cases since a homeomorphism can have no critical points.† (a) Since the slope is positive at all points, period-doubling cannot occur. (b) If the slope is everywhere negative, let us assume that there is a parameter for which the slope is equal to -1.‡ The periodic orbit of prime period two denoted by $\{x_1^*, x_2^*, x_1^*, x_2^*, x_1^*, x_2^*, \ldots\}$ can be expressed as $f(x_1^*) = x_2^*$ and $f(x_2^*) = x_1^*$ or $f(f(x_1^*)) = x_1^*$ and $f(f(x_2^*)) = x_2^*$. In order for the periodic orbit of prime period two to further period-double, the slope of $f(f(\cdot))$ must cross -1. By the chain rule, the slope of $f(f(\cdot))$ can be written as $f'(x_1^*)f'(x_2^*)$. Since this product is always positive, period-doubling cannot occur beyond prime period two. ■

In the next subsection we show that the Poincaré map for a first order buck

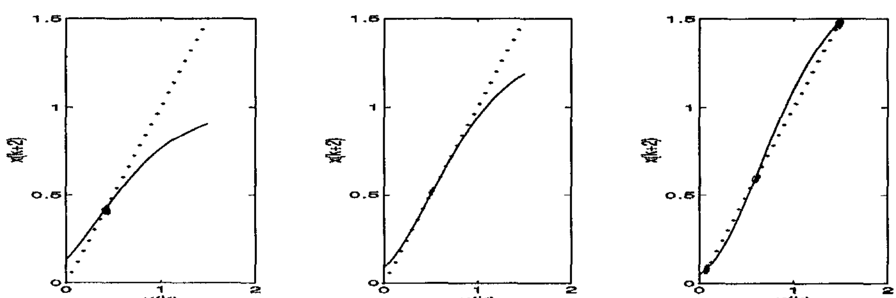

FIG. 8. The second return of a homeomorphic map of the form $x_{k+1} = \lambda e^{-(k_1+k_2x_k)}+k_3$. As the parameter λ is varied, the slope of the fixed point passes through $+1$ and the period-one orbit doubles, leading to three corresponding fixed points, two stable and one unstable.

† A critical point of a function $f\colon \mathbb{R} \to \mathbb{R}$ is defined to be a point x^* where the slope $f'(x^*)$ is equal to 0.

‡ If this is not the case, then period-doubling cannot occur and this will fall into the category defined by (a). Details are given in (**9**).

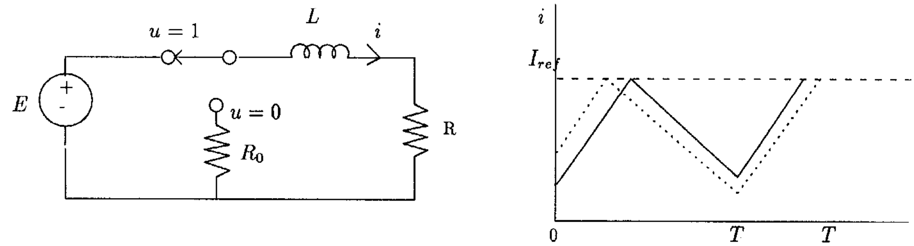

FIG. 9. First order buck under current mode control without compensation ramp. The current waveform corresponding to a duty ratio less than one-half exhibits stable behavior.

converter under current-mode control, without a compensation ramp, is a homeomorphism, and that this explains why it can period-double once, but not again.

4.2.2. *Current mode control of first order buck without compensation ramp.* Current mode controlled DC–DC converters without compensation ramps are known to period-double. The usual analysis in the power electronics literature (**10**, **11**) concludes that period-doubling occurs approximately when the duty cycle is one-half. Here, the duty cycle is the fraction of each cycle that the switch is in the $u = 1$ position. This conclusion can be based on geometric analysis of the current waveform shown in Fig. 9, where the current trajectory is approximated as being piecewise linear. As is evident from the pair of trajectories in Fig. 9, the eigenvalue of the corresponding Poincaré map is negative. This is because the pair of trajectories crosses exactly once during a single period of operation. As may also be evident from the figure, the magnitude of the eigenvalue is less than one, i.e. the trajectories are converging, with duty cycle less than one-half. This situation changes when a single bifurcation occurs with duty cycle of approximately one-half. For duty cycles beyond one-half, the eigenvalue is negative and has magnitude greater than one. For more details on this geometric analysis, see for example (**10**, **11**). The remainder of the subsection develops corresponding algebraic results for the circuit of Fig. 9. The important conclusion here is that the Poincaré map is homeomorphic and only one period-doubling bifurcation is possible.

First, we derive state equations for the circuit. The first order buck converter of Fig. 9 has state equation given by

$$\dot{x}_1 = -u\omega_1 x_1 - (1-u)\omega_2 x_1 + ub_1, \tag{3}$$

where $x_1 = i$ is the inductor current,

$$\omega_1 = \frac{R}{L}, \quad \omega_2 = \frac{R+R_0}{L} \quad \text{and} \quad b_1 = \frac{E}{L}.$$

The input u takes on the values 0 and 1, according to the instantaneous position of the switch as indicated in Fig. 9.

Under normal operation in current mode control, the circuit switches from $u = 0$ to $u = 1$ at the beginning of each period, beginning with the period starting at $t_0 = 0$. The control switches from $u = 1$ to $u = 0$ at time t_{sw} satisfying the intercept constraint

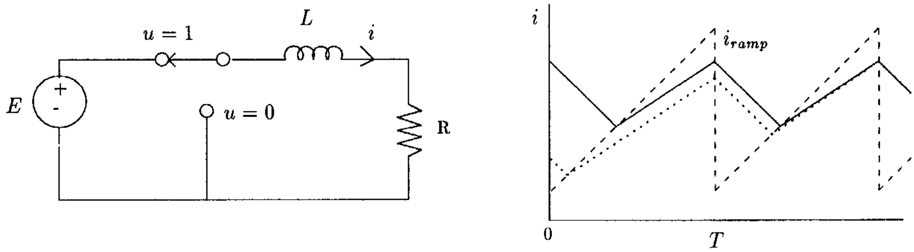

FIG. 10. First order buck under current mode control with compensation ramp.

$$I_{ref} = x_1(t_{sw}) = \left(x_1(t_0) - \frac{b_1}{\omega_1}\right)e^{-\omega_1 t_{sw}} + \frac{b_1}{\omega_1}, \tag{4}$$

as indicated in Fig. 9.

Poincaré map formulation. Next, we use the state equations derived above to derive a Poincaré map for the circuit. Without loss of generality, let $t_0 = 0$ and denote $x_1(0) = x_n$ and $x_1(T) = x_{n+1}$. The solution of the system under $u = 0$ is

$$x_{n+1} = e^{-\omega_2(T-t_{sw})}x_1(t_{sw}). \tag{5}$$

Substituting for t_{sw} from Eq. (4), one obtains the Poincaré map as

$$x_{n+1} = \left[\frac{b_1 - \omega_1 x_n}{b_1 - \omega_1 I_{ref}}\right]^{\omega_2/\omega_1} I_{ref}\, e^{-\omega_2 T}. \tag{6}$$

For $R_0 \ll R$, which implies that $1 < \omega_2/\omega_1 \ll 2$, the Poincaré map is a homeomorphism with negative slope. Applying Lemma H to the circuit, we conclude that the system can period-double to prime period two.

In fact, this Poincaré map does lead to a single period-doubling bifurcation when the parameter b_1 (corresponding to the source voltage) is varied from a large positive value toward zero. Note that we have included the resistance R_0 so that the Poincaré map will yield a unique period-doubled trajectory. With $R_0 = 0$, the Poincaré map turns out to be linear.

4.2.3. *Current mode control of first order buck converter with compensation ramp.* Since the period-doubling bifurcation discussed above is usually considered a hazard in a circuit design, circuit designers often include a stabilizing compensation ramp to avoid this bifurcation. The circuit of Fig. 9 is modified in a number of ways to yield the circuit of Fig. 10. First, we take $R_0 = 0$. Second, the control is implemented in a slightly different manner. Namely, the switch is held in the $u = 0$ position at the beginning of each cycle, until a ramp intercept event triggers the transition to the $u = 1$ position. We use this convention to be consistent with the analysis of this circuit in (**12**). Note the importance of the introduction of a *stabilizing ramp.*

With the relationship between the ramp and the current waveform as shown in Fig. 10, the eigenvalue corresponding to the Poincaré map for this circuit is actually positive. This is a result of the geometry of this diagram where the current trajectory actually crosses the compensation ramp at the intercept point. As such, any pair of trajectories cannot cross, as illustrated in Fig. 10. It is evident from elementary geometric considerations that the corresponding eigenvalue is positive, and hence bounded away from -1. As such, period-doubling is avoided.

Note that this conclusion requires that the current trajectory actually crosses the compensation ramp. As discussed in (**12**), this requires that the compensation ramp be designed with adequate slope to avoid *multiple pulsing*. Multiple pulsing would occur in the implementation of (**12**) if the current waveform were able to cross the compensation ramp more than once per period. To avoid this, the compensation ramp is designed with slope greater than the slope of the current waveform under $u = 1$ for all feasible parameter values. Note that many other current mode control implementations avoid multiple pulsing with the use of a latch.

Poincaré map formulation. The first order buck converter of Fig. 10 analyzed in (**12**), has state equation

$$\dot{x}_1 = -\omega_1 x_1 + u b_1 \tag{7}$$

where $x_1 = i$ is the inductor current, $\omega_1 = R/L$, $b_1 = E/L$ where E denotes the input voltage, and u takes on values 0 and 1 corresponding to the switch position. Under normal operation, the switch transition from $u = 1$ to $u = 0$ occurs periodically with period T beginning at $t = 0$. The system switches from $u = 0$ to $u = 1$ at time t_{sw} satisfying the constraint

$$x_1(t_{sw}) = i_{ramp}(t_{sw}), \tag{8}$$

where $i_{ramp}(t) = i_{min} + (i_{max} - i_{min})F(t/T)$, and $F(x)$ returns the fractional part of x.

Without loss of generality, let $t_0 = 0$ and denote $x_1(0) = x_n$ and $x_1(T) = x_{n+1}$. The state trajectory under $u = 0$ yields

$$x_1(t_{sw}) = \mathrm{e}^{-\omega_1 t_{sw}} x_n, \tag{9}$$

and under $u = 1$ yields

$$x_{n+1} = \left[x_1(t_{sw}) - \frac{b_1}{\omega_1} \right] \mathrm{e}^{-\omega_1 (T - t_{sw})} + \frac{b_1}{\omega_1}. \tag{10}$$

Combining, the Poincaré map is given by

$$x_{n+1} = x_n \mathrm{e}^{-\omega_1 T} + [1 - \mathrm{e}^{-\omega_1 (T - t_{sw})}] \frac{b_1}{\omega_1} \tag{11}$$

with the constraint

$$\mathrm{e}^{-\omega_1 t_{sw}} x_n = i_{min} + \frac{i_{max} - i_{min}}{T} t_{sw}. \tag{12}$$

Even without an explicit expression for t_{sw}, useful information about stability can be obtained by computing the eigenvalue (of the Jacobian) of the Poincaré map given by

$$\frac{dx_{n+1}}{dx_n} = e^{-\omega_1 T}\left[1 - b_1 e^{+\omega_1 t_{sw}} \frac{dt_{sw}}{dx_n}\right] \tag{13}$$

where

$$\frac{dt_{sw}}{dx_n} = \frac{e^{-\omega_1 t_{sw}}}{\omega_1 x_1(t_{sw}) + \dfrac{i_{max} - i_{min}}{T}}. \tag{14}$$

It is clear that, for passive circuit elements, ω_1 is positive and so the quantity $e^{-\omega_1 T}$ always has magnitude less than 1. Therefore, any instabilities are due to non-zero dt_{sw}/dx_n. However for this circuit, even though dt_{sw}/dx_n is non-zero, dx_{n+1}/dx_n always has magnitude less than 1 provided the ramp is designed to avoid *multiple pulsing*. Multiple pulsing could occur if the slope of the current waveform exceeded the slope of the ramp with $u = 1$. Since the maximum value of $\dot{x}_1$ (for the $u = 1$ system) occurs at $t = t_{sw}$, a proper design would ensure that $-\omega_1 x_1(t_{sw}) + b_1 < (i_{max} - i_{min})/T$. Therefore $b_1 e^{+\omega_1 t_{sw}}(dt_{sw}/dx_n) < 1$. Therefore dx_{n+1}/dx_n is always positive and hence the exclusion of period-doubling.

4.3 *Period-doubling cascade to chaos*

Now that the case of power electronic circuits with homeomorphic Poincaré maps has been covered, we move on to DC–DC converters that period-double repeatedly to chaos. The subsection begins with a presentation of a period-doubling cascade normal form, and ends with circuit examples.

4.3.1. *Normal form.* The normal form for period-doubling bifurcations leading to chaos is the logistic map F_λ given below:

$$F_\lambda(x) := \lambda x(1-x), \quad 0 \leqslant x \leqslant 1, \quad 1 \leqslant \lambda \leqslant 4. \tag{15}$$

This *normal form* is only applicable to the case of everywhere differentiable Poincaré maps.

For $1 \leqslant \lambda \leqslant 4$, F_λ maps [0, 1] to [0, 1]. Solving the fixed point equation $F_\lambda(x) = x$ gives the fixed points 0 and $x^*(\lambda) = (\lambda - 1/\lambda)$. for $x^*(\lambda) \in [0, 1]$, we need $\lambda \geqslant 1$. We find also that $d/dx\, F_\lambda(0) = \lambda$ and $d/dx\, F_\lambda(x^*(\lambda)) = 2 - \lambda$. So 0 is always unstable (since $\lambda \geqslant 1$) and $x^*(\lambda)$ is stable *only* for $1 < \lambda < 3$.

At $\lambda_0 = 3$, $d/dx\, F_\lambda(x^*(\lambda_0)) = -1$, so $x^*(\lambda)$ undergoes a pitchfork (period-doubling) bifurcation and becomes unstable for $\lambda \geqslant 3$. Moreover, a stable two-cycle† is born. The two period-two periodic points x_1, x_2 satisfy the equations

$$x_2 = F_\lambda(x_1) = \lambda x_1(1 - x_1) \tag{16}$$

$$x_1 = F_\lambda(x_2) = \lambda x_2(1 - x_2) \tag{17}$$

resulting in

$$x_{1,2} = \frac{1 + \lambda \pm \sqrt{\lambda^2 - 2\lambda - 3}}{2\lambda}. \tag{18}$$

†An m-cycle for a map f is a set of m points $\{x_1, \ldots, x_m\}$ such that $f(x_i) = x_{i+1}$, $1 \leqslant i \leqslant m-1$, and $f(x_m) = x_1$. Hence each x_i is a periodic point of period m for f.

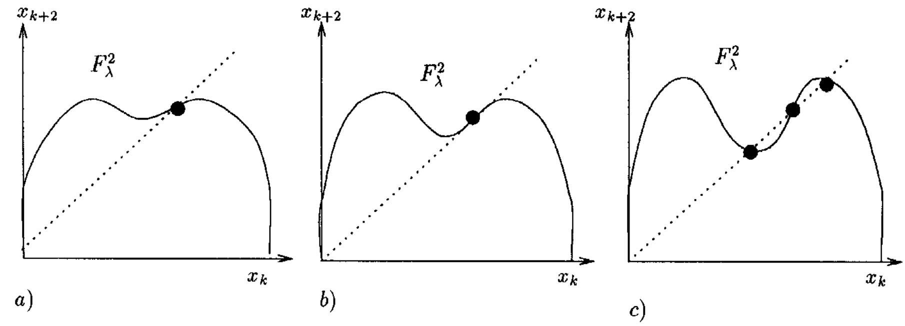

FIG. 11. Logistic map period-doubling for the first time. This is the second return map, x_{k+2} as a function of x_k. The second return map F^2 goes from having one fixed point, corresponding to a stable, period-one orbit, to three fixed points, corresponding to a stable period-two orbit and an unstable period-one orbit, as the parameter λ is increased.

Figure 11 illustrates this first period-doubling bifurcation of the logistic map, occurring at $\lambda = 3$. This figure shows the second return map, which goes from having a single stable fixed point corresponding to a period-one orbit to three fixed points corresponding to the newly unstable period-one orbit and the stable period-two orbit.

Since x_1, x_2 form a two-cycle for the map F_λ, each is a fixed point for the iterated map F_λ^2. Also the term $\lambda^2 - 2\lambda - 3$ in Eq. (18) is negative for $\lambda < 3$, which explains why period-two fixed points do not exist for $\lambda < 3$. Recall that F_λ has a fixed solution given by $x^*(\lambda) = (\lambda - 1)/\lambda$. Initially the attracting set consists of the single point $x^*(\lambda)$ that bifurcates into two points $x_{1,2}(\lambda)$ at $\lambda_1 = 3.0$.

Denote the jth composition of F by F^j. Note, that $\mathrm{d}/\mathrm{d}x\, F_\lambda^2(x_1(\lambda)) = \mathrm{d}/\mathrm{d}x\, F_\lambda^2(x_2(\lambda)) = -1$ when $\lambda = \lambda_2 = 1 + \sqrt{6} = 3.44949\ldots$. So the map F_λ^2 undergoes a period-doubling bifurcation at λ_2. Since both $x_1(\lambda)$, $x_2(\lambda)$ are fixed points for F_λ^2, they lose their stability and bifurcate into four points at λ_2. These four points are *stable* fixed points for the iterated map F_λ^4, and thus are stable periodic points of period four for F_λ. For example, at $\lambda = 3.5$, the steady state solution (or attracting set) cycles among the four values of 0.82694, 0.50088, 0.87500 and 0.38282. On increasing λ further, the number of alternating steady state values increases with 2^n, the interval between successive bifurcation values decreases, and the distance between neighboring periodic points decreases until eventually what looks like a chaotic attracting set appears. This is called a *period-doubling cascade to chaos*.

Next, we present power electronic circuit examples that appear to undergo period-doubling cascades to chaos.

4.3.2. *Second order buck in continuous conduction mode under PWM control.* Unlike the first order buck converter examples, the second order buck converter of Fig. 12 can exhibit more than one period-doubling bifurcation. As outlined below, this circuit has been shown to exhibit the period-doubling route to chaos.

As detailed in (**12**), the state equations describing the operation of the second order buck converter of Fig. 12 are

TABLE I
First eight bifurcation values for the logistic map F_λ

$\lambda_1 = 3.0$	$\lambda_5 = 3.568759\ldots$
$\lambda_2 = 3.449490\ldots$	$\lambda_6 = 3.569692\ldots$
$\lambda_3 = 3.544090\ldots$	$\lambda_7 = 3.569891\ldots$
$\lambda_4 = 3.564407\ldots$	$\lambda_8 = 3.569934\ldots$

$$\dot{x}_1 = -\omega_0 x_2 + u b_1 \tag{19}$$

$$\dot{x}_2 = +\omega_0 x_1 - \omega_1 x_2 \tag{20}$$

where

$$x_1 = i\sqrt{L}, \quad x_2 = v\sqrt{C}, \quad \omega_0 = \frac{1}{\sqrt{LC}} \quad \text{and} \quad \omega_1 = \frac{1}{RC}, \quad b_1 = \frac{E}{\sqrt{L}},$$

and the variables i and v denote the current through L and the voltage across C, respectively.

The control is analogous to that of the current mode controlled buck converter with a compensation ramp, except that an error voltage developed by comparing the capacitor voltage with a reference is the variable used to control the circuit. This is illustrated in Fig. 12.

Poincaré map formulation. Unlike first order DC–DC converters, it is *not* possible to "invert" the $u = 0$ system to solve for switching time t_{sw} when the system transits from the $u = 0$ system to the $u = 1$ system. Instead, extensive numerical simulations were performed in (**12**) to investigate *period-doubling*.

Numerical results from (**12**). The second order buck converter circuit exhibits period-doubling behavior as the amplitude of the input voltage (E) is varied from 15.0 V to 40.0 V. For $E < 25.0$ V the circuit has a stable periodic orbit with period T, which then bifurcates to two (identical in phase space, but shifted in time) stable periodic orbits of period $2T$ at $E \approx 28.0$ V. At $E \approx 32.0$ V the two $2T$ periodic orbits bifurcate to four stable $4T$ periodic orbits and so on. This phenomenon repeats until a stable periodic orbit of period $2^K T$ fills in a dense region on the

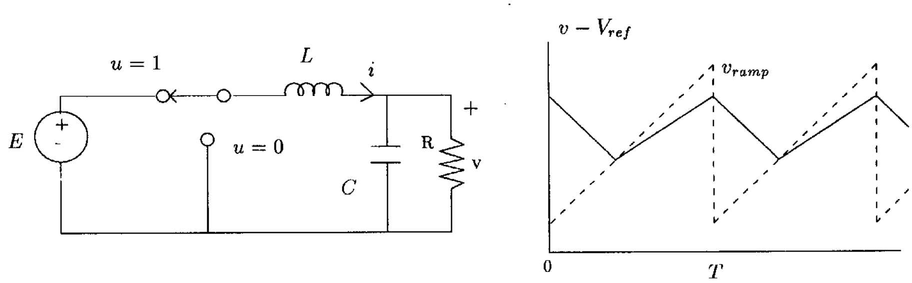

FIG. 12. Second order buck in continuous conduction mode under PWM control.

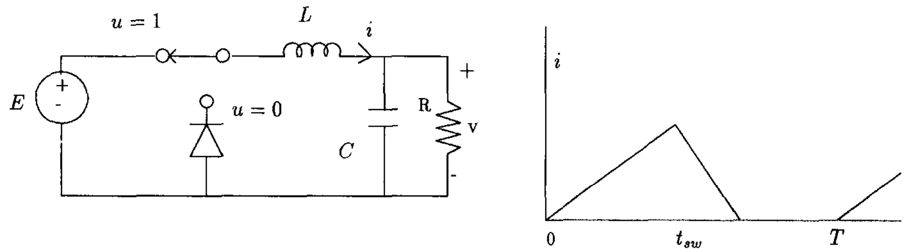

FIG. 13. Second order buck in discontinuous conduction mode.

Poincaré section. For large K, this stable periodic orbit resembles a *chaotic attractor*. These numerical observations are also experimentally confirmed in (**12**). As such, the PWM feedback controlled buck converter appears to exhibit the period-doubling cascade to chaos.

4.3.3. *Second order buck in discontinuous conduction mode.* Another related circuit example exhibiting the period-doubling route to chaos is that of a feedback controlled buck converter operating in discontinuous conduction mode. A circuit model with a typical current waveform is shown in Fig. 13. The circuit is distinguished from the other buck converter examples by the presence of a diode which prohibits the inductor current from reversing. As such, this circuit can exhibit a mode of operation involving three phases: (i) the switch is in the $u = 1$ position, (ii) the switch is in the $u = 0$ position, with the inductor current $i > 0$, and (iii) the switch remains in the $u = 0$ position, with the inductor current $i \equiv 0$. This mode of operation is known as *discontinuous conduction mode* since the inductor current has a period during each cycle where it is identically zero.

One advantage for analysis of this circuit in discontinuous conduction mode is that one only needs to deal with a first order Poincaré map. This route of analysis was taken in (**13**). A nearly identical analysis for a similar boost converter was carried out in (**14**).

The state equations in (**13**) describing the operation of the second order buck converter of Fig. 13 are specified with three phases of operation.

We define

$$x_1 = i\sqrt{L}, \quad x_2 = v\sqrt{C}, \quad \omega_0 = \frac{1}{\sqrt{LC}} \quad \text{and} \quad \omega_1 = \frac{1}{RC},$$

the variables i and v denoting the current through L and the voltage across C respectively and $b_1 = E/\sqrt{L}$, where E is the input voltage. With $u = 1$ the system is described by

$$\dot{x}_1 = -\omega_0 x_2 + b_1 \tag{21}$$

$$\dot{x}_2 = +\omega_0 x_1 - \omega_1 x_2. \tag{22}$$

For $u = 0$ with $x_1 > 0$, the system is modeled by

$$\dot{x}_1 = -\omega_0 x_2 \tag{23}$$

Vol. 331B, No. 6, pp. 957–999, 1994

$$\dot{x}_2 = +\omega_0 x_1 - \omega_1 x_2. \tag{24}$$

When the inductor current reaches zero, the system is described by

$$\dot{x}_1 = 0 \tag{25}$$

$$\dot{x}_2 = -\omega_1 x_2. \tag{26}$$

Poincaré map formulation. Take the sampling times as $t_n = nT$ which coincide with the times at which the circuit is switched from the $u = 0$ to the $u = 1$ configuration. Denote the transition times from $u = 1$ to $u = 0$ as $t_{\mathrm{sw}-n}$. Let Φ_i denote the state transition matrices for the three phases of operation and denote $x(t_n) = [x_1(t_n), x_2(t_n)]^T$. Note that x_1 does not need to be considered as a state variable since the inductor current is identically zero at sampling instants, $x_1(nT) \equiv 0$. When all transition matrices have been computed, we obtain an iterative map of the form

$$x(t_{n+1}) = f(x(t_n), d_n) \tag{27}$$

where d_n is the duty cycle during the nth period, defined as

$$d_n = \frac{t_{\mathrm{sw}-n} - t_n}{T}.$$

An open loop system results if d_n is fixed and a closed loop system results if d_n is dependent on $x(t_n)$. The infinite series representation of the state transition matrices Φ_i are approximated in (**13**) with power series including only up to second order terms, i.e.

$$\Phi_i(\tau) = I + A_i\tau + \tfrac{1}{2}A_i^2\tau^2.$$

Neglecting x_1 since $x_1 \equiv 0$ at all $t = nT$ and letting $y_n = v_c$, a one-dimensional *approximate* Poincaré map is constructed in this fashion and is given by

$$y_{n+1} = My_n + \frac{Nd_n^2 E(E-y_n)}{y_n} \tag{28}$$

where

$$M = 1 - \frac{T}{RC} + \frac{T^2}{2R^2C^2}$$

$$N = \frac{T^2}{2LC}.$$

The *closed loop* system studied in (**13**) is controlled with the feedback law:

$$d_n(y_n) = 0, \quad d_{\mathrm{ref}} - k(y_n - v_{\mathrm{ref}}) < 0$$

$$d_n(y_n) = 1, \quad d_{\mathrm{ref}} - k(y_n - v_{\mathrm{ref}}) > 1$$

$$d_n(y_n) = d_{\mathrm{ref}} - k(y_n - v_{\mathrm{ref}}), \quad \text{otherwise}.$$

The resulting approximate Poincaré map falls into the class of *unimodal* maps (that have one local maximum or minimum), which is well known to exhibit the period-doubling route to chaos. Verification of chaos and period-doubling by computer simulations and by experiment are presented in (**13**).

4.4. *Period-doubling genericity depends upon orbital asymmetry*

In this subsection, we address the question of how likely a power electronic circuit is to period-double by presenting results relating the genericity of period-doubling bifurcations to orbital symmetries. To summarize, though in general period-doubling bifurcations are considered to be generic, they are not generic to orbits with half-cycle symmetry. This sheds light on why it is that power electronic circuits that have been observed to undergo period-doubling bifurcations, such as the examples in this section, do not in general have half-cycle symmetric orbits, though many power electronic circuits do.

4.4.1. *Period-doubling for half-cycle symmetric orbits.* Various *symmetries* in power electronic circuits are detailed in (**15**). These symmetry properties can be used for easing computational effort and for compact model descriptions. Symmetries in power electronic circuits imply that a complete cycle of circuit operation may be composed of a basic pattern that is repeated a certain number of times, with some special transformation of the pattern at each repetition within the cycle. In this subsection, we only focus on deriving Poincaré maps for circuit operations with half-cycle symmetry. Results from (**16**) are used to formulate conditions for period-doubling in power electronic circuits with half-cycle symmetry. The following discussion is extracted from (**15**). Consider the case when the half-cycle Poincaré map corresponding to the first half-cycle of every cycle can be written as

$$x(t_{2k+1}) = f(x(t_{2k})). \tag{29}$$

A number of power electronic circuits with two patterns per cycle (half-wave symmetry) have the property that the evolution in the second half-cycle is governed by the same function, $f(x(\cdot))$, acting on a *transformed* state vector so that the full-cycle Poincaré map can be written as

$$Wx(t_{2k+2}) = f(Wx(t_{2k+1})) \tag{30}$$

where $W^2 = I$, the identity matrix, so that $W = W^{-1}$. The following results are for the symmetry $W = -I$.

Definition

The trajectory of the continuous time trajectory $x^*(t)$ corresponding to a half-cycle symmetric periodic orbit satisfies $x^*(t) = -x^*(t+T/2)$, where T is the period of the periodic orbit. The following results are extracted from (**16**) with minor modifications.

*Lemma S*1

Symmetry breaking of $x^*(t)$ is equivalent to period-doubling of the half-cycle Poincaré map but *not* of the full-cycle Poincaré map.

Vol. 331B, No. 6, pp. 957–999, 1994

Lemma S2

Period-doubling of the full-cycle Poincaré map is equivalent to period-quadrupling of the half-cycle Poincaré map. This is equivalent to a pair of eigenvalues of the half-cycle Poincaré map on the unit circle at $\pm i$.

Lemma S3

Period-quadrupling of the half-cycle map occurs when at least two eigenvalues of the full-cycle Poincaré map are coincident at -1.

Proof of S1, S2, S3: Denote the map from $x(t_0)$ to $x(t_1)$ as $P_{t_0}^{t_1}$. It follows that the full-cycle Poincaré map can be written as $P_{t_0}^{t_0+T}$ and without loss of generality, let $t_0 = 0$. Denote the full-cycle and the half-cycle Poincaré maps as P and P_H respectively, where $P_H = P_0^{T/2}$. The symmetries of $x^*(t)$ are given by

$$x \to -Ix \tag{31}$$

$$t \to t + \frac{T}{2}. \tag{32}$$

The derivation of the half-cycle Poincaré map P_H follows directly from the commutativity relationship:

$$(-I)*P_{T/2}^{T} = P_0^{T/2}*(-I) \tag{33}$$

where $*$ denotes composition. This leads to $P_0^T = (-I*P_0^{T/2})^2$ or $P = (P_H)^2$. Lemmas S1, S2, S3 follow directly from the definitions of the eigenvalues of the Jacobian DP_H of the half-cycle Poincaré map, denoted by μ_i and the eigenvalues of the Jacobian DP of the full-cycle Poincaré map, denoted by λ_i. Lemma S1 implies that only one μ_i is on the unit circle at -1. Lemma S2 follows from $\lambda_i = (\mu_i)^2$. Lemma S3 follows from Lemma S2 and implies that period-doubling for symmetric periodic orbits is an exceptional (*non-generic*) occurrence for single parameter variations. ■

Some circuit examples with half-cycle symmetry. The *series resonant converter* analyzed in **(15)** is an example of a double-ended DC–DC converter, and is known to exhibit *half-cycle symmetry*. The state space is described by $\dot{x} = A_i x + b_i$ where $i = 1, 2$ and $x(t) = [v_C, i_L]^T$. The circuit has the property that $A_1 = A_2$ and $b_1(t, x) = -b_2(t + T/2, -x)$. In the second half-cycle of each cycle, the transformed vector $-x(t)$ satisfies the same set of equations satisfied by $x(t)$ in the first half-cycle. So the circuit satisfies the symmetry analyzed above with the matrix W equal to $-I$, where I is the two by two identity matrix. For details, refer to **(15)**. Also, the thyristor controlled reactor analyzed in **(17)** and detailed in Section V, has periodic orbits that exhibit the $W = -I$ or *half-cycle symmetry*.

V. Bifurcations of Discontinuous Poincaré Maps

5.1. *Introduction*

Poincaré maps of power electronic circuits may be discontinuous. In this section we discuss the simplest type of steady state bifurcation one can find in circuits with discontinuous Poincaré maps, which can lead to a jump phenomenon unlike that

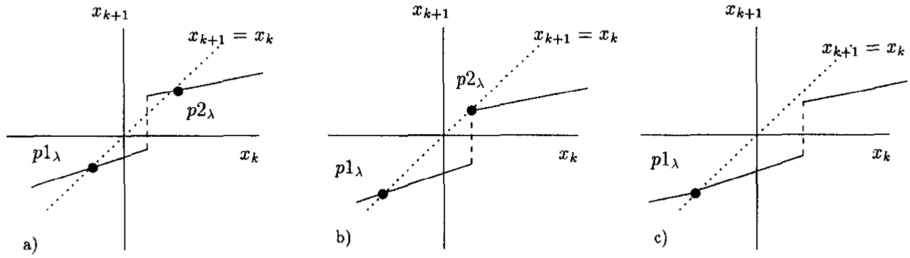

FIG. 14. Discontinuous Poincaré map. (a) At $\lambda = \lambda^*_-$, there are two real fixed points, $p1_\lambda$ and $p2_\lambda$. (b) At $\lambda = \lambda^*$ we approach the edge of the discontinuity. (c) At $\lambda = \lambda^*_+$, the map has only one real fixed point, $p1_\lambda$.

explained in the previous sections. Also, other types of bifurcations one might expect to find in such systems are suggested, as discussed in (**18**). We end the section with a thyristor circuit example (**17**), and conjecture that it is the presence of state controlled switches combined with certain kinds of fairly typical switching control functions that produce discontinuous Poincaré maps and their associated bifurcations.

5.1.1. *Geometry-simple models.* Figure 14 illustrates a simple, one-dimensional, discontinuous Poincaré map undergoing what we will call a *discontinuity bifurcation* as a parameter is varied. For some range of parameter values, this map has two fixed points, $p1_\lambda$ and $p2_\lambda$, as shown in Fig. 14(a). The two fixed points are on disconnected segments of the map. As a parameter is varied, the intersection of one of the segments and the diagonal approaches the discontinuity, as shown in Fig. 14(b). If the parameter is varied beyond the discontinuity value, only a single map segment will intersect the diagonal, and the map will no longer have two fixed points, but only one, $p1_\lambda$, as shown in Fig. 14(c).

An example of such a map is

$$x_{k+1} = P_\lambda(x_k) = \begin{cases} 0.5x_k + 1 + \lambda & \text{if } x_k > 0 \\ 0.5x_k - 1 + \lambda & \text{if } x_k < 0. \end{cases}$$

This map has a single discontinuity, occuring at $x_k = 0$. For $|\lambda| < 1$, the map has two stable fixed points, and for $|\lambda| > 1$, the map has a single stable fixed point. Discontinuity bifurcation parameter values are $\lambda = +1$ and $\lambda = -1$.

Parameterized solution sets of discontinuous maps are fundamentally different from those of differentiable or continuous maps. One basic difference is that varying a parameter can cause a real fixed point to either appear or disappear, and this change in the number of fixed points of a map is not necessarily accompanied by the merging of multiple fixed points, a continuum of fixed points, or by an escape to infinity, as it would for a continuous map. For example, discontinuous maps can, with the variation of a parameter, go from having an even number of fixed points to an odd number of fixed points, without an occurrence like a change in degree or an escape to infinity. This is impossible for continuous maps. Another basic difference between discontinuous and analytic maps, which are infinitely differentiable, is the connection between real and complex solution space. For an

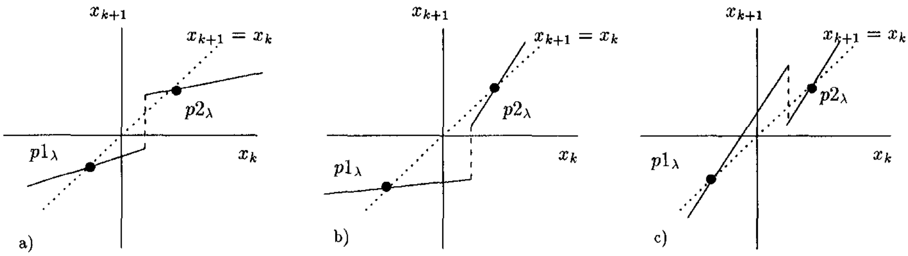

FIG. 15. Possible stability combinations of discontinuous Poincaré maps. (a) Both $p1_\lambda$ and $p2_\lambda$ are stable. (b) The fixed point $p1_\lambda$ is stable, and $p2_\lambda$ is unstable. (c) Both fixed points are unstable.

analytic map, the number of real fixed points (assume map degree constant) can only change by factors of two, and the "disappearing" real solutions of analytic maps can be thought of as appearing in complex space once they coalesce at a bifurcation. For example, $x_{k+1} = x_k^2 + \lambda$ has two real fixed points for $\lambda < 0$ and no real fixed points for $\lambda > 0$, but it does have two *complex* solutions for $\lambda > 0$ connected to the real root paths in parameter space by the bifurcation point.

Naturally, *eigenvalues* do *not* signal an approaching discontinuity bifurcation. This is because if the map is not continuous, the eigenvalues of its linearization, where defined, won't be continuous either. Unlike bifurcations of continuous and differentiable maps, all stability combinations of fixed points on either side of a discontinuity are possible, as illustrated in Fig. 15. Fixed point combinations can be stable–stable, stable–unstable, or unstable–unstable.

Next, we briefly describe jump phenomena of discontinuous maps, which can occur in power electronic circuits like the one described in the next subsection.

5.1.2. *Jump phenomena.* If both fixed points shown in Fig. 14 are stable, and the associated circuit happens to be in the steady state corresponding to the fixed point $p2_\lambda$ prior to the bifurcation, the discontinuity bifurcation will lead to *jump* behavior in the circuit, from the fixed point $p2_\lambda$ to the fixed point $p1_\lambda$ with the variation of a parameter.

5.1.3. *Other bifurcations due to discontinuities.* The authors of (**18**) explore a special class of discontinuous one-dimensional Poincaré maps and their dynamics. The class of maps studied in (**18**) is like the simple discontinuous maps in this section, in that it is composed of piecewise continuous maps with a countable number of discontinuities, but unlike in that the map slopes on the continuous sections are monotonic and have magnitude greater than one, so no stable periodic orbits can exist. These maps are characterized by semi-periodic intervals, stochastic attractors, and ergodic invariant measures.

An open topic of study is whether power electronic circuits with discontinuous Poincaré maps, such as the thyristor controlled reactor of the next subsection or other switched circuits satisfying the conditions of Subsection 5.3, can have more complicated dynamics like those described in (**18**) and the references therein.

Next, we analyze a simple power electronic circuit with a discontinuous Poincaré

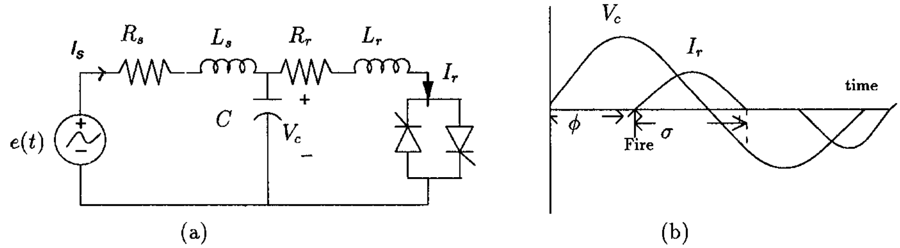

FIG. 16. (a) Thyristor circuit. Single phase static VAR. (b) Classical operation.

map and show that the map discontinuities lead to jump phenomenon with the variation of a parameter.

5.2 *Circuit example* (*thyristor controlled reactor*)

Unlike the switched converter circuits analyzed in Section IV, the thyristor controlled reactor (TCR), explored in (**17**), undergoes bifurcations in an open loop configuration. In this section we review some of the derivations and bifurcation observations discussed in (**17**), and interpret them in terms of *map discontinuities* and their associated bifurcations. We also contribute additional simulation and bifurcation results, and generalize to other switched circuits in Subsection 5.3.

5.2.1. *Circuit operation.* The thyristor controlled reactor (TCR) circuit explored in (**17**) is shown in Fig. 16(a). It consists of an R–L–C circuit driven by a sinusoidal source, with a switching element consisting of two oppositely poled thyristors. Each thyristor is modeled as an ideal switch that turns on upon receiving a firing pulse provided its anode–cathode voltage is positive, and turns off when the current passing through the device goes to zero. The firing pulses are applied periodically, with a period equal to that of the sinusoidal source driving the circuit, and a phase of ϕ with respect to either the voltage across the capacitor, $v_c(t)$ (assuming the waveform is close to sinusoidal), or to the sinusoidal source $e(t)$. The bifurcation studies of (**17**) are done with the phase ϕ as an *open loop* control parameter, where ϕ is measured with respect to the source voltage $e(t)$.

Figure 16(b) illustrates the typical operation of a thyristor controlled reactor circuit. As explained in (**17**), the gray line denotes the (assumed) sinusoidal voltage across the capacitor, $V_c(t)$, and the black line represents the current I_r. After a ϕ radian delay from the capacitor voltage, the positively poled thyristor is fired. It remains on and conducts positive current until the thyristor current goes to zero. Then it remains off until the thyristor is fired again 2π radians (the normalized period of the source input) later, at $\phi+2\pi$.

The negatively poled thyristor is fired with a $\phi+\pi$ delay from the capacitor voltage. If the circuit is operating properly, the thyristor current will be zero upon firing the pulse, and the thyristor will conduct negative current and remain on until the thyristor current goes to zero. This thyristor then remains off until it is fired again 2π radians later, at $\phi+3\pi$.

This type of circuit has two types of operation: continuous conduction and discontinuous conduction. If the delay ϕ coincides with the peak capacitor voltage (at $\phi = \pi/2$), then the current conduction through the thyristors is continuous. For delays ϕ that do not coincide with the peak capacitor voltage, the current conduction is discontinuous, meaning that the thyristor current remains zero over an open interval of time, as in Fig. 16(b). The conduction times σ can range from 0 to π, and depend on the firing delay ϕ.

5.2.2. *State equations.* The authors of (**17**) formulate the TCR state equations as follows. The system state vector $x(t)$ consists of the thyristor current I_r, the capacitor voltage V_c, and the source current I_s:

$$x(t) = \begin{pmatrix} x_1(t) \\ x_2(t) \\ x_3(t) \end{pmatrix} = \begin{pmatrix} I_r(t) \\ V_c(t) \\ I_s(t) \end{pmatrix}.$$

The system input $e(t)$ is assumed to be periodic with period T. During the conduction time of either thyristor, the system dynamics are described by the linear differential equations

$$\dot{x} = Ax + Be \tag{34}$$

where

$$A = \begin{pmatrix} -R_r L_r^{-1} & L_r^{-1} & 0 \\ -C^{-1} & 0 & C^{-1} \\ 0 & -L_s^{-1} & -R_s L_s^{-1} \end{pmatrix}$$

and

$$B = \begin{pmatrix} 0 \\ 0 \\ L_s^{-1} \end{pmatrix}.$$

During the off time of each thyristor, the state is constrained to the plane $I_r = 0$ of zero thyristor current. In the off time, the system state vector $y(t)$ consists of the capacitor voltage and the source current:

$$y(t) = \begin{pmatrix} V_c(t) \\ I_s(t) \end{pmatrix}$$

and the system dynamics are given by the linear system

$$\dot{y} = PAP'y + PBe \tag{35}$$

where P is the projection matrix

$$P = \begin{pmatrix} 0 & 1 & 0 \\ 0 & 0 & 1 \end{pmatrix}.$$

The two-dimensional state vector $y(t)$ is the projection $y = Px$ of the full conduction state vector $x(t)$ onto the zero thyristor current plane.

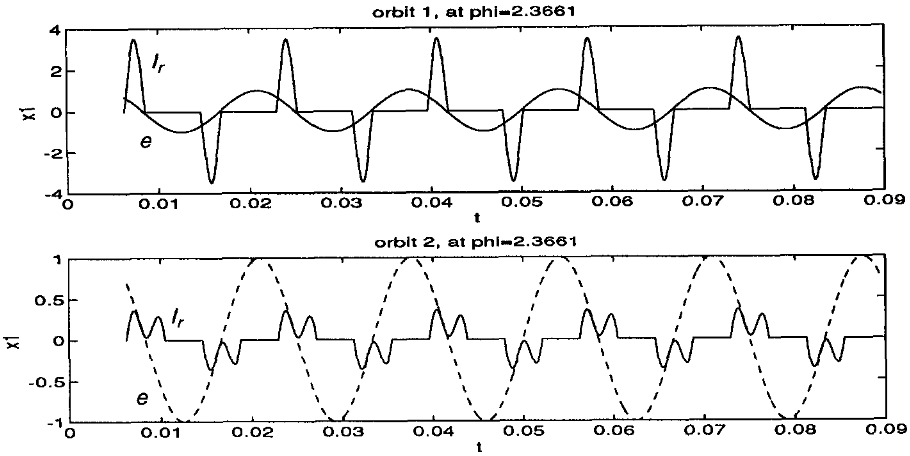

FIG. 17. Two periodic orbits at the same value of $\phi(\phi = 2.3661)$, orbit 1 and orbit 2. These plots show I_r, the current through the thyristor, and $e(t)$, the source voltage, as a function of time.

The dynamics of the circuit are thus described by alternating systems of linear differential equations, from the *on* system described by Eq. (34), to the *off* system described by (35), restricted to the $I_r = 0$ plane, and then back again. Switching from the on to the off system occurs at switch times t_s satisfying the condition $I_r(t_s) = 0$. Switching from the off to the on system occurs upon receiving a firing pulse from the periodic pulse train. As will be shown, the characteristics of the nonlinear equation $I_r(t_s) = 0$ determine the bifurcation properties of this circuit. For further details on circuit operation and equation derivation, see (**17**).

5.2.3. *Multiple orbits/jump phenomenon.* Here, we summarize simulation results from (**17**) and from our own MATLAB programs. We study periodic steady states of the circuit shown in Fig. 16(a) with component values $L_s = 0.195$mH, $R_s = 0.9$mΩ, $L_r = 1.66$mH, $R_r = 31.3$mΩ and $C = 1.5$mF as specified in (**17**), and an input source of $e(t) = \sin wt$, with $w = 2\pi\dot{6}0$ rad/s.

Our MATLAB programs employ a shooting method (**8**) over the period $T = w/(2\pi)$ to identify periodic steady states of the circuit for a given delay ϕ of the thyristor firing pulses with respect to the input source. We varied ϕ from 0 to π radians, and calculated periodic orbits for each chosen value of ϕ. See (**17**) for a derivation of the Jacobian that we used in our program.

We found, in agreement with results in (**17**), a *single* stable periodic orbit for values of ϕ ranging from $\phi = 0$ to $\phi \approx \pi/2$, and from $\phi \approx 2.374$ to $\phi \approx \pi$, and *two* stable periodic orbits for ϕ ranging from $\phi \approx \pi/2$ to $\phi \approx 2.374$. Figure 17 shows thyristor current plotted against time for the two stable periodic orbits at $\phi = 2.3661$, which we will call orbits 1 and 2. Notice that orbit 1 is large in current magnitude, but with a relatively small conduction time σ, while orbit 2 has a small peak value but a larger conduction time σ. For a fixed value of ϕ, half symmetric waveforms like these may be identified by their conduction times σ. This is because

Vol. 331B, No. 6, pp. 957–999, 1994

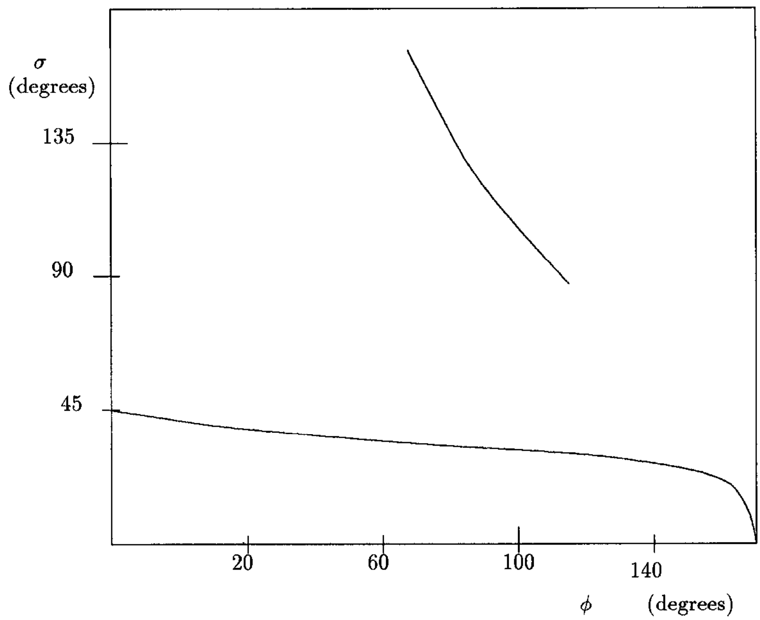

FIG. 18. Current conduction time σ as a function of the delay ϕ.

if the homogenous component† of the Poincaré map equation is nonsingular, as it is for this circuit, two distinct orbits at the same value of ϕ must have different conduction times.

Figure 18 illustrates a plot of the current conduction time for each calculated steady state as a function of the delay ϕ. The figure makes clear the number of orbits calculated for each value of ϕ, the relationship of these orbits to one another, and the relationship of these orbits to those at neighboring values of ϕ. Observe that there appear to be two continuous solution sets, one above the other, and that orbit 1 in Fig. 17, with its small conduction time, is in the solution set with small conduction times ($\sigma < \pi/4$). This orbit is one of a continuum of stable orbits that exists as ϕ is swept over the entire range, from 0 to π. This means that if the circuit is in a steady state anywhere along this path of periodic solutions, operating for example in orbit 1, then an infinitesimal perturbation in the delay time ϕ will lead to an infinitesimal deformation of the periodic orbit. Along this solution path of orbits with relatively small conduction times, the steady state is a *continuous* function of the delay time ϕ over the allowable range of ϕ.

Orbit 2, with its relatively large conduction time $\sigma > \pi/3$, is on the abbreviated looking solution path visible from $\phi \approx \pi/2$ to $\phi \approx 2.374$. Unlike the path of solutions with smaller conduction times, this path of solutions does not extend continuously from $\phi = 0$ to $\phi = \pi$, but seems to have a starting point near $\phi = \pi/2$

†The Poincaré map derived in (**17**) may be written $y_{n+1} = A(t_{s1}, t_{s2})y_n + g(t_{s1}, t_{s2}, y_n, e)$, where the "homogenous" component of the map, denoted by $A(\cdot)$, consists of products of matrix exponentials and functions of switch times t_{si}.

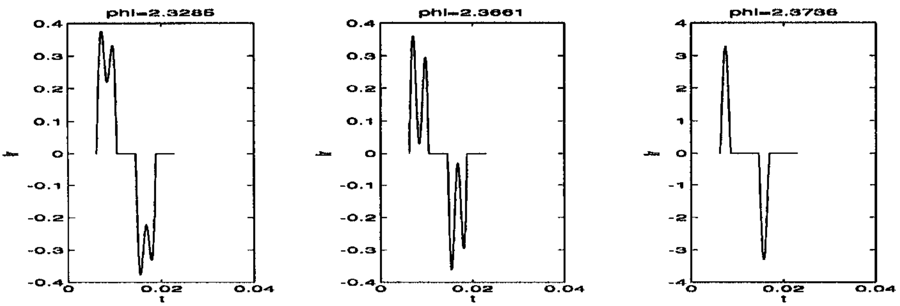

FIG. 19. Steady state current I_r vs. time, for varying delays. The stable periodic steady state jumps from an orbit with a large conduction time σ to one with a small conduction time σ past $\phi = 2.3661$.

and an endpoint near $\phi = 2.374$. If the circuit is operated in a steady state along this path at a value of ϕ that is not near one of the endpoints of the path, then a small perturbation in ϕ will result in a small deformation in the periodic steady state, as is the case anywhere along the continuous, smaller conduction solution path including orbit 1. However, if the circuit is operated in the large conduction orbit at $\phi = 2.374$, and ϕ is perturbed, say to $\phi = 2.3743$, then the trajectory will jump to a new steady state that is not just a mild deformation of the steady state at $\phi = 2.374$. Rather, it will jump to a new steady state that is markedly different from the pre-perturbation orbit, one with a small conduction time on the other solution path, as shown in Fig. 18. This *jump phenomenon* is also shown in the MATLAB plots of stable periodic orbits at different values of ϕ, in Fig. 19, and in the state space projections of these orbits in Fig. 20.

The leftmost endpoint of this solution set, near $\phi \approx \pi/2$, marks the value of ϕ at which the circuit operates in continuous conduction mode. This path does not continue to the left because an attempt at continuing the path for $\phi < \pi/2$ results in a misfire, and only normal circuit operation is considered. For more on misfires, see (**17**).

5.2.4. *Interpretation*: *return map discontinuity*. Steady state jump phenomena with the variation of a parameter is common for nonlinear circuits. Typically, jump phenomenon is associated with a cyclic fold bifurcation, as described in Subsection 3.1 for differentiable Poincaré maps, and in Appendix A for continuous Poincaré maps.

Tracing out the eigenvalues of the Poincaré map in the neighborhood of the bifurcation reveals that no eigenvalue approaches $+1$, as it would in the case of a generic cyclic fold bifurcation of a differentiable Poincaré map. The eigenvalues near the jump are at $0.8232 \pm 0.075i$. Because no eigenvalue approaches the unit circle at the jump, the authors of (**17**) conclude that the jump is not due to a typical, differentiable, cyclic fold bifurcation.

That still leaves open the possibility of the jump being caused by a cyclic fold bifurcation of a continuous, but not everywhere differentiable map, as discussed in the Appendix. Such a bifurcation would *not* be signaled by an eigenvalue

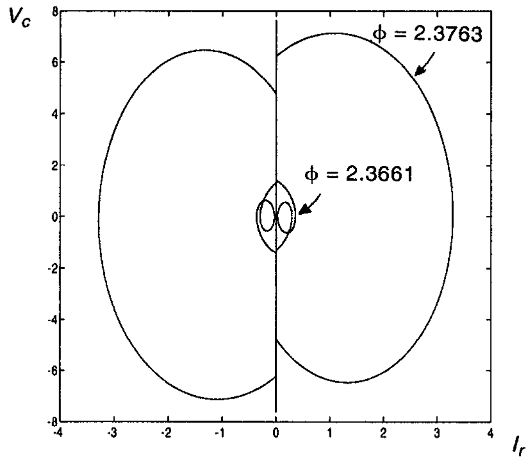

FIG. 20. Current I_r vs. capacitor voltage, for $\phi = 2.3661$, before the jump, and for $\phi = 2.3763$, after the jump. This figure shows two superimposed stable orbits of the TCR at different values of delay ϕ corresponding to the orbits in the first and third panels of Fig. 19.

approaching $+1$, so the observation that the system eigenvalues do not approach the unit circle does not preclude a cyclic fold bifurcation of a continuous, non-differentiable map. However, the thyristor circuit in question cannot have any *unstable* T-periodic steady states, as was shown in (**17**). Since, as discussed in the Appendix, a generic cyclic fold bifurcation of a continuous, but not everywhere differentiable map involves the coalescing of an unstable and a stable or unstable orbit, a generic CFB of a non-differentiable map must also be ruled out for this circuit.

Now that typical cyclic fold bifurcations of differentiable and continuous maps have been ruled out for the thyristor circuit, we look to the possibility that the jump behavior is caused by a discontinuity in the map. A numerical investigation of the Poincaré map, as illustrated in Fig. 21, reveals this to be the case. The jump behavior appears to be caused by a discontinuity bifurcation, much like the simple geometric model presented in the beginning of the section. We show that the Poincaré map is discontinuous, and link the discontinuity to what the authors of (**17**) call a *switch time bifurcation*. We show that these switch time bifurcations determine the Poincaré map discontinuity pattern, and that waveforms in continuous regions of the map, for a given value of ϕ fall into equivalence classes.

5.2.5. *A discontinuous return map*. The system Poincaré map is obtained by sampling the state $x(t)$ every T seconds, where T is the period of the input sinusoid $e(t)$. To reduce the map to two dimensions, the trajectory is sampled at $t_k = t_{\rm on}+kT = \phi T/(2\pi)+kT$, $k = 0, 1, 2, \ldots$, at the arrival of the thyristor firing pulses. At times t_k the thyristor current $x_1(t_{\rm on}) = I_r(t_{\rm on}) = 0$ under normal operating conditions. Since $x_1 = 0$ at all sample values, the Poincaré map may be defined as

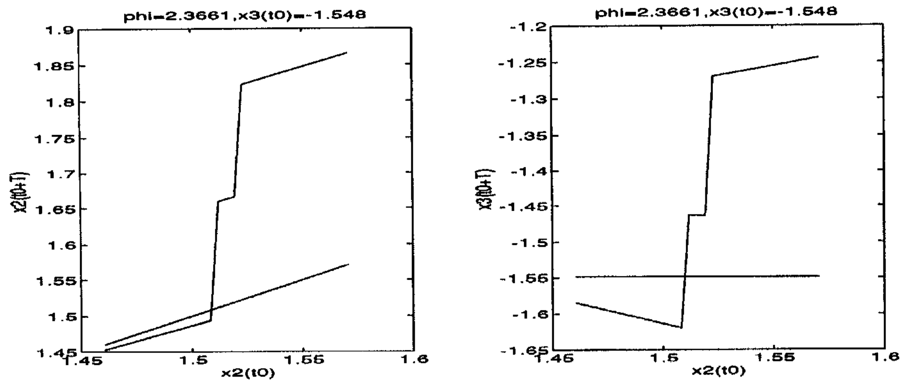

FIG. 21. Double discontinuity in map. (a) $x_2(T+t0)$ as a function of $x_2(t0)$. (b) $x_3(T+t0)$ as a function of $x_2(t0)$. In both cases, $x_3(t0)$ is fixed at -1.5489, and ϕ is fixed at 2.3661. The discontinuities occur at $x_2(t0) \approx 1.5083$ and $x_2(t0) \approx 1.5211$.

a two-dimensional mapping $P_\phi : y_0 \to y_T$, where $y_0 = y(t_{\text{on}}) = (x_2(t_{\text{on}}), x_3(t_{\text{on}}))$ and $y_T = y(t_{\text{on}}+T) = (x_2(t_{\text{on}}+T), x_3(t_{\text{on}}+T))$.

An analytic expression for the Poincaré map P_ϕ is defined in (**17**). Because the Poincaré map P_ϕ maps $\mathbb{R}^2 \to \mathbb{R}^2$, it is somewhat difficult to visualize. As an aid, we first think of the map as an interconnected pair of maps from $\mathbb{R}^2 \to \mathbb{R}$, one from the $(x_2(t_{\text{on}}), x_3(t_{\text{on}}))$ plane to $x_2(t_{\text{on}}+T)$ and the other from the $(x_2(t_{\text{on}}), x_3(t_{\text{on}}))$ plane to $x_3(t_{\text{on}}+T)$. Then, to further simplify, we trace a *curve* through the $(x_2(t_{\text{on}}), x_3(t_{\text{on}}))$ plane and look at $x_2(t_{\text{on}}+T)$ and $x_3(t_{\text{on}}+T)$, respectively, as a function of the values of $(x_2(t_{\text{on}}), x_3(t_{\text{on}}))$ along the curve. We call such a procedure, which is equivalent to intersecting the Poincaré map with a vertical surface, *slicing* the map.

Figure 21 (a),(b) shows a slice of the Poincaré map, at a fixed delay of $\phi = 2.3661$. These are MATLAB plots, obtained by simulating the circuit over a period T (numerically integrating the state equations (34), (35) over T seconds), from t_{on} to $t_{\text{on}}+T$, starting from chosen initial conditions $x_2(t_{\text{on}})$ and $x_3(t_{\text{on}})$ along the line defining the map slice. The line through the $(x_2(t_{\text{on}}), x_3(t_{\text{on}}))$ plane defining the slice shown in Fig. 21 (a),(b) is parallel to the $x_2(t_{\text{on}})$ axis, with $x_3(t_{\text{on}})$ held constant at -1.5489.

Figure 21 (a),(b) shows $x_2(t_{\text{on}}+T)$ and $x_3(t_{\text{on}}+T)$ as a function of $x_2(t_{\text{on}})$, with $x_3(t_{\text{on}})$ held at -1.5489. Notice that there are *two* discontinuities on the slice of map shown, one at $(x_2(t_{\text{on}}), x_3(t_{\text{on}})) \approx (1.5083, -1.5489)$, and the other at $(x_2(t_{\text{on}}), x_3(t_{\text{on}})) \approx (1.5211, -1.5489)$. Other numerically obtained slices reveal similar discontinuities, and, for a fixed ϕ, the map discontinuities projected onto the $(x_2(t_{\text{on}}), x_3(t_{\text{on}}))$ plane make a jagged pattern. Thus, we have observed numerically that the Poincaré map is indeed discontinuous. See also Fig. 22.

Next, we will review the switch time bifurcations discussed in (**17**) and discuss their relationship to the numerically observed map discontinuities, and follow with a discussion of the previously described jump phenomenon in the circuit. As will

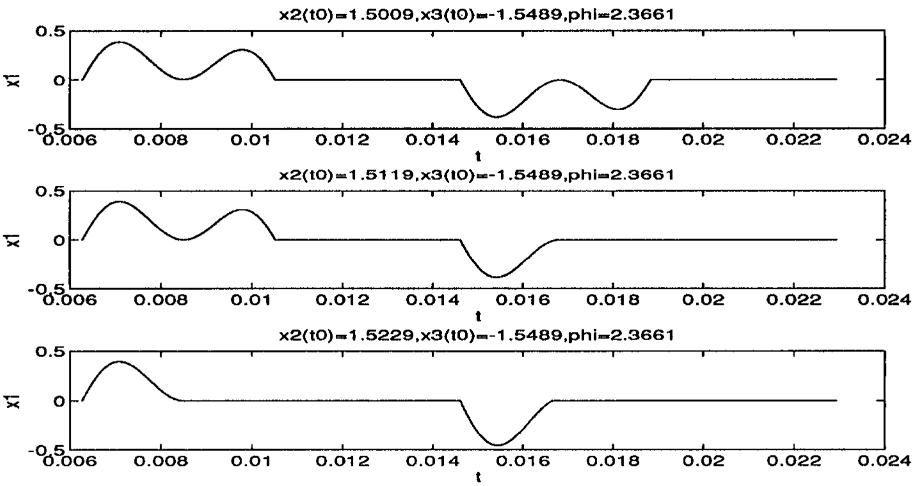

FIG. 22. Waveforms corresponding to three regions in the Poincaré map bridged by the two discontinuities. (a) Current I_r in nearly half-wave symmetric region with large conduction time. (b) Current I_r in asymmetric region. (c) Current I_r in nearly half-wave symmetric region with small conduction time. Note that each waveform differs from the other by a switch time bifurcation.

be seen, the map discontinuities can be both numerically observed and analytically explained.

5.2.6. *Switch time bifurcations.* In this section we show that the map discontinuities observed numerically in the previous subsection are due to the fact that thyristor switch off time t_s is a *discontinuous function* of both *initial condition* $x(t_0)$ and *delay* ϕ.

Recall that the thyristor circuit switches from an *on* to an *off* state when the current I_r goes to zero. When the thyristor conducts current, Eq. (34) describes the system dynamics, and the state trajectory is given explicitly by

$$x(t+t_0) = e^{At}(P'y(t_0)+\int_0^t e^{-A\tau}Bu(\tau+t_0)\,d\tau) \quad \textbf{(17)}.$$

Setting $t_0 = t_{\text{on}}$, the time at which a pulse is fired, and $t = \sigma$, the thyristor conduction time, leads to an expression of the switching condition as

$$I_r(t_s) = I_r(t_{\text{on}}+\sigma) = [1 \ \ 0 \ \ 0]x(t_{\text{on}}+\sigma) = 0$$

where t_s is the switch-off time of the thyristor.

Since the *on* state of the thyristor circuit corresponds to a linear ordinary differential equation with a sinusoidal input, and the matrix A has complex conjugate eigenvalues, the state trajectory of system (34), if allowed to continue uninterrupted by the switching of the thyristor upon satisfaction of the condition

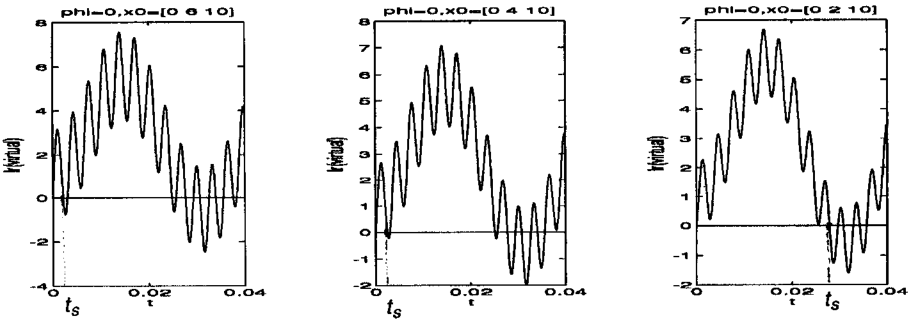

FIG. 23. Virtual thyristor current as a function of initial condition $x(0)$, with fixed delay ϕ. (a) At $x(0) = (0, 6, 10)$ the first zero crossing t_s, which serves as a switch time in the complete circuit, is around $t_s \approx 0.005$. (b) At $x(0) = (0, 4, 10)$, t_s has only shifted slightly, since t_s varies continuously with the initial condition in the neighborhood. (c) By $x(0) = (0, 2, 10)$, t_s has jumped in a switch time bifurcation. Switch time t_s is not a continuous function of the initial conditions in general.

$I_r(t_s) = 0$, would resemble a *modulated sine wave*. Figures 23 and 24 show the thyristor current I_r of the *on* system, extended far beyond the first zero crossing, where the actual circuit would switch into the *off* state, for various initial conditions and firing delays. We look at these extended curves, called *virtual* waveforms in (**17**), to better understand how the switching time t_s depends on initial conditions and the firing delay ϕ.

Figure 23(a) shows the virtual I_r current curve with initial conditions $x_2(0) = 6$ and $x_3(0) = 10$ and a delay $\phi = 0$. Examine the location of the switch time t_s, the first zero crossing of the virtual current. It is around $t \approx 0.005$, and occurs before the first local minima of the function. Figure 23(b) shows the virtual current curve with the initial conditions perturbed to $x_2(0) = 4$ and $x_3(0) = 10$. In this case a perturbation in the initial conditions, from $x_2(0) = 6$ to $x_2(0) = 4$, leads to a fairly small change in the switch time t_s, because this perturbation lies within the set

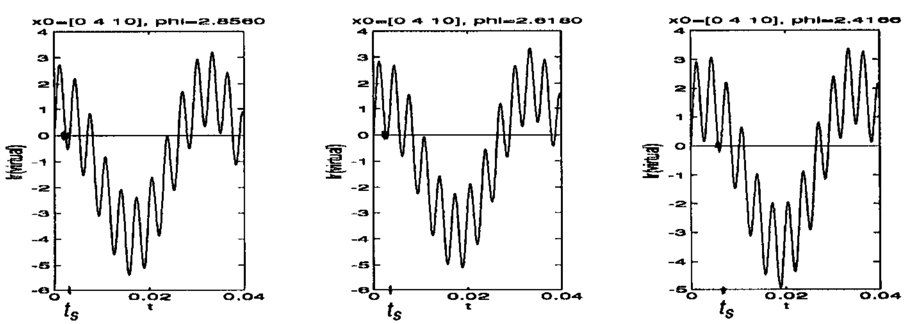

FIG. 24. Virtual thyristor current as a function of delay ϕ, with fixed initial condition $x(0) = (0, 4, 10)$. (a) Delay $\phi = 2.856$. (b) Delay $\phi = 2.618$. (c) Delay $\phi = 2.4166$. Notice the switch time bifurcation. The first zero crossing, t_s, is not a continuous function of ϕ.

where switch time is a continuous function of the initial condition. The switch time t_s of the circuit at the new initial condition occurs before the first local minima of the virtual current, as was the case for $x_2(0) = 6$ and $x_3(0) = 10$.

However, because of the oscillatory nature of the virtual current, the switch time t_s is not, in general, a continuous function of the initial conditions $x_2(0)$ and $x_3(0)$, or the delay ϕ. Figure 23(c) shows the virtual current with initial conditions perturbed to $x_2(0) = 2$ and $x_3(0) = 10$. In this case a perturbation in the initial conditions leads to a large instantaneous jump in the switch time t_s. This jump is referred to as a switch time bifurcation in (**17**). Notice that the switch time t_s with $x_2(0) = 2$ and $x_3(0) = 10$ does not occur before the first local minima of the virtual current, as was the case at the two previously discussed initial condition values. Rather, the new t_s occurs after many local minima of the function, around $t \approx 0.025$. Decreasing $x_2(0)$ has the effect of raising the first minima of the virtual current until it no longer intersects the $I_r = 0$ axis, upon which t_s, the first current zero crossing, will jump to what was the ith zero crossing of the current ($i \neq 1$). The actual bifurcation value occurs when the local minima exactly intersects the zero axis, at $\mathrm{d}I_r(t)/\mathrm{d}t = 0$ at the switching time $t = t_s$, as discussed in (**17**). Figure 24 shows virtual current as a function of time for fixed initial conditions and varying delay times ϕ. As can be seen, the switch time t_s is a *discontinuous function of firing delay* ϕ as well as the initial state of the circuit.

Switch time bifurcations account for discontinuities in the Poincaré map, like the ones shown in Fig. 21 (and also Figs 26, 27, and 28). As formalized in Subsection 5.3 for the general case of switched circuits, of which the TCR is one, if a change in initial condition $\Delta x(t_0)$ leads to a jump in the switch time t_s, then the state $x(t_0+T)$ will also jump, and this implies a discontinuity in the Poincaré map of the circuit. Analytically, this discontinuity set is defined by the switch bifurcation condition $\mathrm{d}I_r(t^*)/\mathrm{d}t = 0$, $t^* = t_s$.

In summary, it can be established that the Poincaré map of the TCR circuit is discontinuous, and that the discontinuities arise because thyristor switch-off times t_s are discontinuous functions of state $x(t_0)$ and firing pulse delay ϕ. To illustrate, Fig. 22 shows a sample waveform from each of the three continuous map segments shown in the discontinuous Poincaré map of Fig. 21. Notice that they are qualitatively different, and, as expected, each differs from the other by a switch time bifurcation.

5.2.7. *Steady state jump phenomenon in terms of discontinuity.* In Subsections 5.2.5 and 5.2.6 we established that the Poincaré map of the TCR is discontinuous, and drew connections between the thyristor switch-off time jump phenomena and the Poincaré map discontinuities. In this subsection, we return to the steady state jump phenomenon described previously and shown in Figs 19 and 20, and explain it in terms of Poincaré map discontinuities.

First, it should be noted that the presence of a discontinuous Poincaré map does not in itself imply that the circuit will undergo a steady state bifurcation akin to the simple discontinuity bifurcation presented in Subsection 5.1, where a stable fixed point intersects a map discontinuity with the variation of a parameter. Among other things, for a discontinuity bifurcation to occur, a fixed point of the Poincaré map must intersect the map discontinuity at a parameter value *within* the allowable

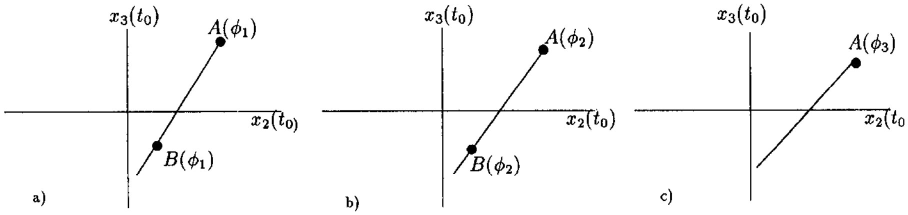

FIG. 25. Defining Poincaré map slices by tracing a line through the equilibrium points at given values of ϕ.

range. Also, another stable fixed point must exist. Therefore, the existence of a discontinuous return map is a necessary, but not sufficient condition for the occurrence of a discontinuity bifurcation of a periodic steady state with the variation of a circuit parameter. The remainder of this subsection is devoted to showing that the thyristor controlled reactor under discussion does indeed undergo a discontinuity bifurcation, and that it is this bifurcation which accounts for the jump phenomenon described in Subsection 5.1.2.

Recall from Subsection 5.2.5 that one way of examining an otherwise hard to visualize Poincaré map $P_\phi: \mathbb{R}^2 \to \mathbb{R}^2$ is to slice it by tracing a line through the $(x_2(t_{\rm on}), x_3(t_{\rm on}))$ plane and plotting $x_2(t_{\rm on}+T)$ and $x_3(t_{\rm on}+T)$ corresponding to the points traced out along the line, respectively. The values $x_2(t_{\rm on}+T)$ and $x_3(t_{\rm on}+T)$ above each point are obtained by simulating the TCR circuit over one period, from $t_{\rm on}$ to $t_{\rm on}+T$, using a point $(x_2(t_{\rm on}), x_3(t_{\rm on}))$ as an initial condition.

Because the object of this section is to observe how the number and placement of periodic orbits and map discontinuities vary with ϕ in the neighborhood of the observed jump, we show slices of the Poincaré map defined by tracing lines through the $(x_2(t_{\rm on}), x_3(t_{\rm on}))$ plane that connect two stable fixed points at given values of ϕ, as shown in Fig. 25, for values of ϕ approaching the jump value, and then slightly beyond. To make the discontinuities easier to see, we plot $x_2(t_{\rm on}+T)-x_2(t_{\rm on})$ as a function of $x_2(t_{\rm on})$ and $x_3(t_{\rm on}+T)-x_3(t_{\rm on})$ as a function of $x_3(t_{\rm on})$ along the lines shown in Fig. 25 at different values of ϕ. We call this representation a *difference map*.

Figures 26–28 show slices of the Poincaré difference map at different values of ϕ. These slices are designed to give information on the number and placement of Poincaré map fixed points, and the relative locations of discontinuities, as a function of ϕ. Notice the change in shape of the map as ϕ is increased. As will be described in detail in the next paragraphs, the fixed point denoted by a B in the plots approaches, and then intersects a neighboring discontinuity, and this leads to the loss of that fixed point and a discontinuity bifurcation. We start off by examining Fig. 26.

Figure 26 shows a slice of the difference map at $\phi = 2.3661$ defined by the line $x_3(t0) = 2.3243x_2(t0)-4.8278$ through the $(x_2(t_0), x_3(t_0))$ plane as represented in Fig. 25(a). This line passes through the two fixed points $A = (x_2, x_3) = (6.3446, 9.9189)$ and $B = (x_2, x_3) = (1.4108, -1.5487)$, sample points of the two periodic orbits shown in Fig. 17, marked by an A and a B in Figs 26 and 25(a). Figure

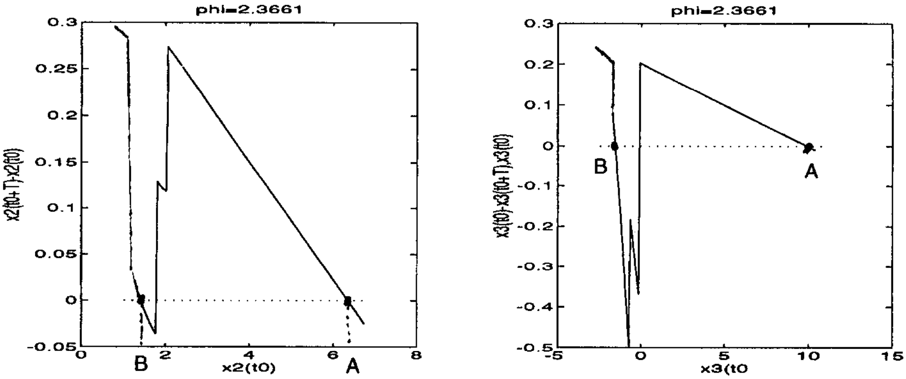

FIG. 26. Slice of Poincaré difference map, for $\phi = 2.3661$ and $x_3(t0) = 2.3243x_2(t0) - 4.8278$. (a) $x_2(t0+T) - x_2(t0)$ as a function of $x_2(t0)$. (b) $x_3(t0+T) - x_3(t0)$ as a function of $x_3(t0)$. Notice triple discontinuity, and two periodic orbits at $(x_2(t0), x_3(t0)) = (6.3446, 9.9189)$ and $(1.4108, -1.5487)$.

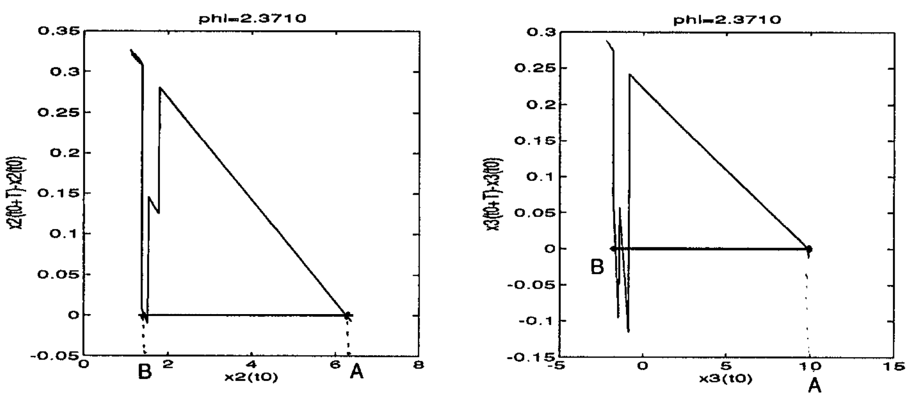

FIG. 27. Slice of Poincaré difference map, for $\phi = 2.3710$ over $x_3(t0) = 2.3586x_2(t0) - 4.9338$. (a) $x_2(t0+T) - x_2(t0)$ as a function of $x_2(t0)$. (b) $x_3(t0+T) - x_3(t0)$ as a function of $x_3(t0)$. Notice triple discontinuity, and two periodic orbits at $(x2, x3) = (6.2723, 9.7651)$ and $(x2, x3) = (1.4408, -1.6472)$.

26 shows MATLAB plots of $x_2(t_{on}+T) - x_2(t_{on})$ as a function of $x_2(t_{on})$ and $x_3(t_{on}+T) - x_3(t_{on})$ as a function of $x_3(t_{on})$ along this line in the $(x_2(t_0), x_3(t_0))$ plane. Notice that the portion of the difference map slice shown has *three* discontinuities, one just before the fixed point $B = (1.4108, -1.5487)$, and two between the Poincaré map fixed points B and $A = (6.3446, 9.9189)$. Each discontinuity corresponds to a switch time bifurcation, so waveforms with initial conditions taken from each of the contiguous sections of the map separated by a discontinuity will differ in shape much like the waveforms of Fig. 22.

Figure 27 shows a slice of the difference map at $\phi = 2.371$ defined by the line $x_3(t0) = 2.3586x_2(t0) - 4.9338$ through the $(x_2(t_0), x_3(t_0))$ plane as represented in

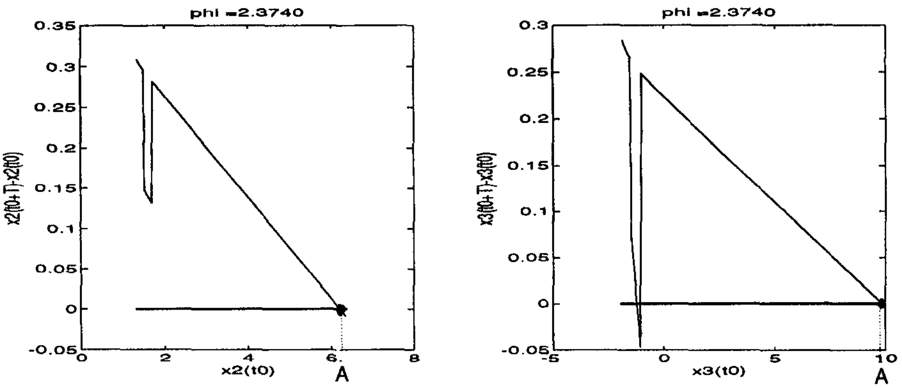

FIG. 28. Slice of Poincaré difference map, for $\phi = 2.374$ over $x_3(t0) = 2.3615x_2(t0) - 5.0637$. (a) $x_2(t0+T) - x_2(t0)$ as a function of $x_2(t0)$. (b) $x_3(t0+T) - x_3(t0)$ as a function of $x_3(t0)$. Notice double discontinuity, and single periodic orbits at $(x_2(t0), x_3(t)) = (6.3446, 9.9189)$ and $(6.2279, 9.6709)$.

Fig. 25(b). This line passes through the two Poincaré map fixed points $A = (x2, x3) = (6.2723,\ 9.7651)$ and $B = (x2, x3) = (1.4408,\ -1.6472)$, sample points of the two periodic orbits at $\phi = 2.371$, marked by an A and a B in Figs 27 and 25(b). Once again, Fig. 27 shows MATLAB plots of $x_2(t_{\text{on}}+T) - x_2(t_{\text{on}})$ as a function of $x_2(t_{\text{on}})$ and $x_3(t_{\text{on}}+T) - x_3(t_{\text{on}})$ as a function of $x_3(t_{\text{on}})$. Observe that the difference map slice shown has three discontinuities, as it did at $\phi = 2.3661$, but that increasing the delay ϕ from $\phi = 2.3661$ to $\phi = 2.371$ results in a decrease in the *distance* between the first and second discontinuity shown, on either side of the fixed point $B = (1.4408,\ -1.6472)$. The Poincaré map fixed point B approaches a neighboring discontinuity.

As the delay ϕ is increased beyond $\phi = 2.371$ the discontinuities on either side of the fixed point B continue to approach the fixed point, until, at $\phi \approx 2.374$, the Poincaré map no longer has two fixed points, but just one, as shown in Fig. 28. The fixed point B coalesces with a discontinuity, and is annihilated. A discontinuity bifurcation much like the simple model described in Subsection 5.1 occurs, and the circuit, if operating in the periodic steady state corresponding to fixed the point B before ϕ is perturbed, jumps to the orbit corresponding to the fixed point A, as shown in Figs 19 and 20 and in the difference map progression shown in Figs 26, 27, and 28.

In summary, Poincaré map discontinuities occur at initial conditions $(x_2(t_0), x_3(t_0))$ and delays ϕ at which the state trajectory of the TCR undergoes switch time bifurcations, and the jump phenomenon discussed earlier and shown in Figs 19 and 20 is explained by a discontinuity bifurcation, wherein a stable fixed point intersects a Poincaré map discontinuity, and the state trajectory previously in the steady state corresponding to the fixed point B approaches the stable fixed point beyond the discontinuity, A.

Vol. 331B, No. 6, pp. 957–999, 1994

5.3. *Generalization: switched circuits with discontinuous maps*

The thyristor controlled reactor circuit discussed in the previous section is an example of a cyclically operated power electronic circuit modeled by state controlled ideal switches in a linear network. The authors of (**15**) represent such circuits in a uniform way, as a succession of LTI state space equations of the form

$$\mathrm{d}x(t)/\mathrm{d}t = A_i x(t) + B_i u_{k,i}(t), \quad t_k + T_{k,i-1} < t < t_k + T_{k,i}, \tag{36}$$

one for each of N switch configurations in the kth cycle, where $T_{k,0} = 0$ and $t_{k+1} = t_k + T_{k,N}$. Thus $T_{k,N}$ is the duration of the kth cycle. The N-vector

$$T_k = \begin{bmatrix} T_{k,1} \\ \vdots \\ T_{k,N} \end{bmatrix} \tag{37}$$

is defined to be the transition time vector. This N-vector represents the transitions that occur when the system state reaches particular boundaries or *threshold conditions*, which includes thyristors turning off (the threshold condition being zero thyristor current) or diodes turning on (the threshold condition being zero diode voltage) or diodes turning off (the threshold condition being zero diode current). The ith threshold condition can be written as $c_i(x(t_k), p_k, T_k) = 0$, where p_k is an independent controlling parameter. In the case of the TCR, p_k is ϕ_k (the kth firing angle that turns on the thyristor), $x(t_k)$ is the 2-tuple of initial conditions, $[V_c(t_k), I_s(t_k)]$ and T_k is the transition time vector. In compact notation, these constraints can be written as an N-vector constraint equation given by

$$c(x(t_k), p_k, T_k) = \begin{bmatrix} c_1(\ldots) \\ \vdots \\ c_N(\ldots) \end{bmatrix} = 0. \tag{38}$$

A sufficient condition for discontinuous Poincaré maps. We can now state precise conditions for a Poincaré map to have discontinuities in terms of the *constraint equation*. Denoting $x(t_k)$ as x_k, the Poincaré map is expressed as $x_{k+1} = f(x_k, T_k)$ with the constraint $c = 0$ and the Jacobian as

$$\left[\frac{\partial f}{\partial x_k}\right] + \left[\frac{\partial f}{\partial T_k}\right]\left[\frac{\partial T_k}{\partial x_k}\right].$$

Rewrite $[\partial T_k/\partial x_k]$, using the implicit function theorem, as

$$\left[\frac{\partial T_k}{\partial x_k}\right] = -\left[\frac{\partial c}{\partial T_k}\right]^{-1}\left[\frac{\partial c}{\partial x_k}\right]. \tag{39}$$

Therefore a *sufficient* condition for discontinuities in the Poincaré map is that the matrix $[\partial c/\partial T_k]$ be *rank deficient*. In other words, small changes in an initial condition of the Poincaré map (Δx_k) results in discontinuous changes in the transition time vector (ΔT_k) which in turn causes discontinuous changes (Δx_{k+1}) in the next iterate of the Poincaré map. ■

This jump in T_k is called a switching time bifurcation in (17). Although switching time bifurcations cause discontinuities in the Poincaré map, we make a distinction between switching time bifurcations and *steady state jump bifurcations* of discontinuous Poincaré maps. Since steady state jumps occur when fixed points collide with the discontinuity surfaces, the presence of switching time bifurcations are necessary but not sufficient for the occurence of steady state jump phenomena in discontinuous Poincaré maps.

VI. Summary

This paper studied various bifurcations of periodic orbits in power electronic circuits: cyclic fold bifurcations, period-doubling bifurcations, and bifurcations due to Poincaré map discontinuities. We focused on circuits operating under closed-loop control and/or containing nonlinear reactive components.

Section III contains an exploration of cyclic fold bifurcations and the associated resonant jump phenomenon in circuits containing saturable reactors. Section IV gives a comprehensive overview of period-doubling phenomena in closed-loop DC–DC conversion circuits. We studied circuits with homeomorphic and unimodal Poincaré maps, those that period-double a single time and those that period-double repeatedly in a cascade to chaos. This section ends with a result relating non-genericity of a period-doubling bifurcation to half-wave orbital symmetry.

An interesting feature of power electronic circuits is that they may have Poincaré maps that are continuous but not everywhere differentiable, or discontinuous. In Section V we studied, in detail, bifurcation behavior in a thyristor controlled VAR compensator. We showed that this circuit has a discontinuous Poincaré map, and analyzed the steady state bifurcation in terms of the discontinuities. We showed that the Poincaré map discontinuities are a product of circuit switch time jumps, and distinguished between transient behavior related to these switch time jumps and the observed steady state jump phenomenon. We then presented general conditions for a switched circuit to have a discontinuous Poincaré map. The paper ends with an appendix, in which concepts underlying cyclic fold bifurcations for the case of a continuous but not everywhere differentiable map are developed.

References

(1) R. J. Duffin, "Impossible behavior of nonlinear networks", in "Proc. Symp. Nonlinear Circuit Analysis", pp. 124–138, Polytechnic Inst. of Brooklyn, NY, 1953.

(2) D. H. Wolaver, "Fundamental Study of DC to DC Conversion Systems", Ph.D. Thesis, EECS Dept., MIT, 1969.

(3) S. R. Sanders, "On limit cycles and the describing function method in periodically switched circuits", *IEEE Trans. Circuits & Syst.*, Vol. 40, pp. 564–572, September 1993.

(4) J. Guckenheimer and P. Holmes, "Nonlinear Oscillations, Dynamical Systems, and Bifurcations of Vector Fields", Springer-Verlag, New York, 1983.

(5) J. B. Deane and D. C. Hamill, "Instability, subharmonics, and chaos in power electronic systems", *IEEE Trans. Power Electr.*, Vol. 5, pp. 260–268, July 1990.

Vol. 331B, No. 6, pp. 957–999, 1994

(6) M. Hasler and J. Neirynck, "Nonlinear Circuits", Artech House Inc., Norwood, MA, 1986.
(7) L. O. Chua, M. Hasler, J. Neirynck and P. Verburgh, "Dynamics of a piecewise-linear resonant circuit", *IEEE Trans. Circuits & Syst.*, Vol. CAS-29, pp. 535–546, August 1982.
(8) K. Kundert, J. White and A. Sangiovanni-Vincentelli, "Steady-State Methods for Simulating Analog and Microwave Circuits", Kluwer, Boston, 1990.
(9) R. L. Devaney, "An Introduction to Chaotic Dynamical Systems", Benjamin/Cummings, Menlo Park, CA, 1986.
(10) R. D. Middlebrook, "Modeling current-programmed buck and boost regulators", *IEEE Trans. Power Electr.*, Vol. 4, pp. 36–52, January 1989.
(11) G. C. Verghese, C. A. Bruzos and K. N. Mahabir, "Averaged and sampled-data models for current mode control: a re-examination", "PESC '89 Record. 20th Annual IEEE Power Electronics Specialists Conference", Vol. 1, pp. 484–491, 1989.
(12) J. B. Deane and D. C. Hamill, "Analysis, simulation and experimental study of chaos in the buck converter", "PESC '90 Record. 21st IEEE Power Electronics Specialists Conference", pp. 491–498, 1990.
(13) C. K. Tse, "Chaos from a buck switching regulator operating in discontinuous mode", *Int. J. Circuit Theo. Appl.*, Vol. 22, pp. 263–278, July–August 1994.
(14) C. K. Tse, "Flip bifurcation and chaos in three-state boost switching regulators", *IEEE Trans. Circuits & Syst. I: Fund. Theo. Appl.*, Vol. 41, pp. 16–23, 1994.
(15) G. C. Verghese, M. E. Elbuk and J. G. Kassakian, "A general approach to sampled-data modeling for power electronic circuits", *IEEE Trans. Power Electr.*, Vol. PE-1, pp. 76–89, April 1986.
(16) J. W. Swift and K. Wiesenfeld, "Suppression of period-doubling in symmetric systems", *Phys. Rev. Lett.*, Vol. 52, pp. 705–708, February 1994.
(17) S. G. Jalali, I. Dobson and R. H. Lasseter, "Instabilities due to bifurcation of switching times in a thyristor controlled reactor", "PESC '92 Record. 23rd IEEE Power Electronics Specialists Conference", pp. 546–552, 1992.
(18) A. N. Sharkowvsky and L. O. Chua, "Chaos in some 1-D discontinuous maps that appear in the analysis of electrical circuits", *IEEE Trans. Circuits & Syst. I: Fund. Theo. Appl.*, Vol. 40, pp. 722–732, October 1993.

Appendix A. Cyclic Folds, Continuous Poincare Maps

Poincaré maps of power electronic circuits may not be everywhere differentiable because of the presence of state controlled switches. In this appendix we discuss cyclic fold bifurcations of circuits with Poincaré maps that are continuous, but only piecewise differentiable.

While it is still true that if the point $p_\lambda \in \tilde{x}_\lambda$ is a fixed point of the map P_λ ($p_\lambda = P_\lambda(p_\lambda)$), then the eigenvalues of the linearization of the differentiable map P_λ at p_λ, $\mu_i \in \mu(DP_\lambda(p_\lambda))$, where defined, reflect the stability of the fixed point p_λ and its corresponding periodic orbit $\tilde{x}_\lambda$, it is not true that they necessarily serve to signal the occurrence of a bifurcation. As in the everywhere differentiable case, if no eigenvalue of the linearized Poincaré map (where defined) is on the unit circle ($|\mu_i| \neq 1, \forall i$), the periodic orbit $\tilde{x}_\lambda$ is hyperbolic. However, because eigenvalues can change their values discontinuously, the condition $|\mu_i| = 1$ for some parameter value is not required for an orbit to bifurcate. Thus, a cyclic fold bifurcation of a continuous but not everywhere differentiable Poincaré map may not correspond to a single eigenvalue $\mu_i \in \mu(DP_\lambda)$ passing through $+1$ transversally, as it does in the differentiable case discussed in the previous section. Also, the requirement (of differentiable maps) that one of

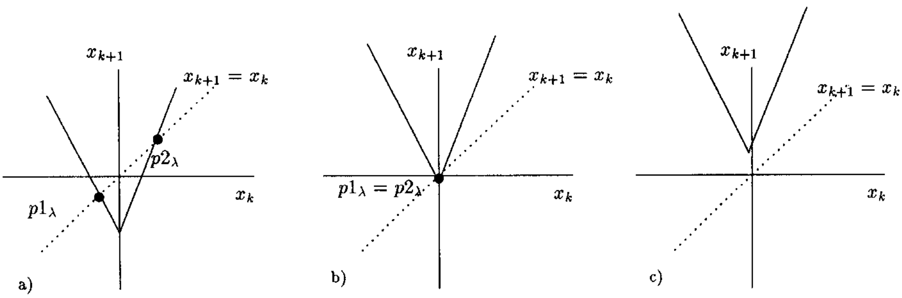

FIG. 29. Piecewise linear model of generic CFB for continuous but not everywhere differentiable Poincaré maps. (a) At $\lambda = \lambda^*_-$, there are two solutions. (b) At $\lambda = \lambda^*$ the two solutions coalesce in a CFB. (c) At $\lambda = \lambda^*_+$, the map has no solutions.

the coalescing orbits be stable and the other unstable does not hold for non-differentiable maps. Next, we look at simple geometric models to explore the possibilities.

Geometry/simple models

Figure 29 illustrates a simple continuous, piecewise differentiable Poincaré map undergoing a cyclic fold bifurcation. An example of such a map, differentiable everywhere except at $x_k = 0$, is as follows:

$$x_{k+1} = P_\lambda(x_k) = 2|x_k| + 1.1x_k + \lambda. \tag{40}$$

As in the case of everywhere differentiable maps, a continuous piecewise differentiable map like $x_{k+1} = P_\lambda(x_k)$ undergoing a CFB will have a range of parameter values λ at which the map has two real distinct fixed points [Fig. 29(a)], a parameter value at which the map has a real double fixed point [Fig. 29(b)], and a range of parameters at which the map has no real fixed points [Fig. 29(c)]. The map $x_{k+1} = P_\lambda(x_k) = 2|x_k| + 1.1x_k + \lambda$ has two real fixed points for $\lambda < 0$, no real fixed points for $\lambda > 0$, and a double root $p1 = p2 = 0$ at $\lambda = 0$. As in the differentiable case, the parameter value at which the two fixed points coalesce and disappear is called the *cyclic fold bifurcation* point.

Two of the main differences between generic CFBs of differentiable maps and those of continuous, non-differentiable maps like $x_{k+1} = P_\lambda(x_k)$ are in the relationship between the eigenvalues of the linearized Poincaré map and the presence of a CFB, and the potential stability combinations of fixed points undergoing a CFB.

Unlike the case of differentiable maps, continuous, piecewise differentiable maps may undergo a cyclic fold bifurcation without any warning from the system eigenvalues. For example, the eigenvalue of the map $x_{k+1} = 2|x_k| + 1.1x_k + \lambda$ linearized about a fixed point p_λ is $2\text{sign}(p_\lambda) + 1.1$ (assuming $p_\lambda \neq 0$), where $\text{sign}(x) = 1$ if $x > 0$ and $\text{sign}(x) = -1$ if $x < 0$. If $p_\lambda > 0$, then the eigenvalue $\mu = 3.1$, while if $p_\lambda < 0$ the eigenvalue $\mu = -0.9$. As the parameter λ is increased from a negative value to zero, the two fixed points move together and coalesce at $\lambda = 0$. However, the eigenvalues of the two orbits remain at $\mu = 3.1$ and $\mu = -0.9$ during the approach, and do not reflect the coming cyclic fold bifurcation. At the cyclic fold bifurcation point $\lambda = 0$, the Poincaré map is not differentiable, so the eigenvalue is not defined at the bifurcation point. This is in contrast to the differentiable case, in which an eigenvalue of the coalescing fixed points approaches $+1$ as the cyclic fold bifurcation point is approached. This is a significant difference, and should be kept in mind when interpreting numerical experiments meant to identify bifurcations of circuits and other

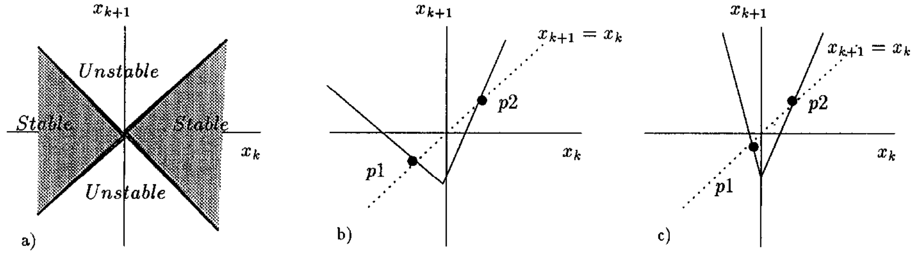

FIG. 30. Stability combinations for CFBs of continuous but not everywhere differentiable Poincaré maps. (a) Stability regions. (b) CFB joining a stable orbit, $p1$, and an unstable orbit, $p2$. (c) CFB joining two unstable orbits.

dynamical systems that can have non-differentiable Poincaré maps, such as those found in power electronic circuits.

Figure 30(b),(c) show the two possible stability configurations of orbits undergoing a generic cyclic fold bifurcation. Figure 30(b) shows the "typical" configuration of a stable fixed point $p1$ and an unstable fixed point $p2$ joined in parameter space by a cyclic fold bifurcation point. Our simple map $x_{k+1} = 2|x_k| + 1.1x_k + \lambda$ is such an example, as the eigenvalues of the two fixed points are $\mu = 3.1$ and $\mu = -0.9$, corresponding to an unstable orbit and a stable orbit, respectively. However, if we modify the map slightly to get a new map,

$$x_{k+1} = 2|x_k| + 0.9x_k + \lambda \tag{41}$$

then the situation changes. The map still undergoes a cyclic fold bifurcation at $\lambda = 0$, but the eigenvalues are now $\mu = 2.9$ and $\mu = 1.1$, which both correspond to unstable orbits. This configuration, where two distinct unstable orbits meet in a cyclic fold bifurcation with the variation of a parameter, is illustrated in Fig. 30(c).

This case differs sharply from the differentiable map case, which has continuous eigenvalues around a cyclic fold, necessarily serving to connect a stable and an unstable orbit. At a cyclic fold bifurcation a differentiable map has an eigenvalue $\mu = +1$. Eigenvalue continuity dictates that as the bifurcation point is approached, the eigenvalues of the two coalescing fixed points must be $\mu = +1+\varepsilon$ and $\mu = +1-\varepsilon$, those of an unstable and a stable fixed point. Once again, it is the fact that continuous, piecewise differentiable Poincaré maps have eigenvalues that can vary discontinuously with the parameter that leads to significant differences between the properties of cyclic fold bifurcations of the two map classes.

The third possible stability configuration, that of two distinct stable orbits meeting at a cyclic fold bifurcation, cannot occur for continuous maps (with transversal bifurcations representable by a one-dimensional model), differentiable or not. Figure 30(a) shows a graphical representation of the stability regions of a fixed point, assumed in the diagram to be at the origin. The regions marked stable (unstable) are meant to signify the range of slopes of the map at the fixed point corresponding to a stable (unstable) fixed point; those with magnitudes that are smaller (larger) than one. Notice that in order for a map to have a cyclic fold bifurcation, one of the two fixed points must have a slope that is greater than $+1$, and this precludes the possibility of two stable orbits meeting in a CFB.

One more variation of a cyclic fold bifurcation that is possible for a continuous piecewise differentiable Poincaré map but not for a differentiable Poincaré map is illustrated in Fig.

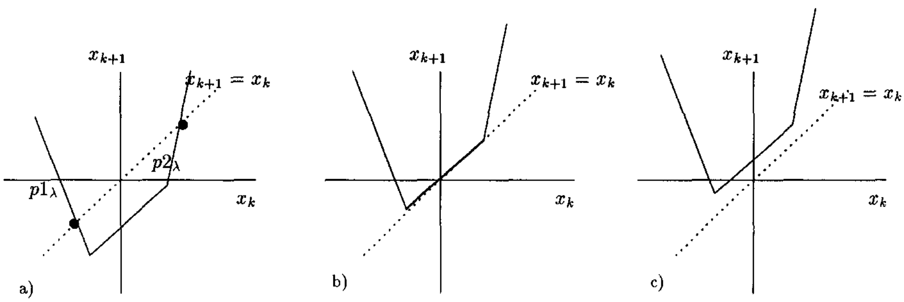

FIG. 31. Model of a non-generic CFB for continuous, piecewise linear Poincaré maps. (a) At $\lambda = \lambda^*_-$, there are two solutions. (b) At $\lambda = \lambda^*$ there is a continuum of solutions. (c) At $\lambda = \lambda^*_+$, the map has no solutions.

31. This is the case where the map has a linear component of slope $+1$ connected to other segments that together form a convex hull. As in the previously discussed cases, a map like this one will have a range of parameter values λ at which the map has two real distinct fixed points [Fig. 31(a)], and a range of parameters at which the map has no real fixed points [Fig. 31(c)]. However, in this case the parameter value at which the two orbits "disappear" does not correspond to a double fixed point of the map. Rather, there will be a *continuum* of orbits linking two distinct orbits, with a range of initial values directly corresponding to the set of fixed points along the segment colinear with the diagonal, as shown in Fig. 31(b). This type of CFB is non-generic, because it is unlikely that a piecewise linear segment of a Poincaré map will have a slope of one and coincide with the diagonal.

Vol. 331B, No. 6, pp. 957–999, 1994